

# **Design and Development of Smart Battery Thermal and Power Management System for PV-Battery- Hydrogen Generation System**

Submitted in partial fulfilment of the requirements of the degree of

**Master of Technology  
Sustainable Energy Generation and Storage Technologies**

by

**Tatipamula Chakrapani  
(24CHM3R02)**

As part of the Dissertation report under the guidance of

**Dr. Leela Manohar Aeshala  
Associate Professor**



**DEPARTMENT OF CHEMICAL ENGINEERING  
NATIONAL INSTITUTE OF TECHNOLOGY WARANGAL  
TELANGANA, INDIA-506004**

2025

## **Approval Sheet**

This summer internship Work entitled by Tatipamula Chakrapani is approved for the degree of Master of Technology in the specialisation of Sustainable Energy Generation and Storage Technologies.

### **Examiners**

### **Supervisor (s)**

### **Chairman (Program Coordinator)**

**Date** \_\_\_\_\_

**Place:**

## **Declaration**

I declare that this written submission represents my ideas in my own words and where others' ideas or words have been included, I have adequately cited and referenced the original sources. I also declare that I have adhered to all principles of academic honesty and integrity and have not misrepresented or fabricated or falsified any idea/data/fact/source in my submission. I understand that any violation of the above will be cause for disciplinary action by the Institute and can also evoke penal action from the sources which have thus not been properly cited or from whom proper permission has not been taken when needed.

**Name of the student:**

**Roll No.:**

**Date:**

## **Certificate**

This is to certify that the Dissertation work entitled “*Design and Development of Smart Battery Thermal and Power Management System for PV-Battery System-Hydrogen Generation System*” is a Bonafide record of work carried out by “*Mr. Tatipamula Chakrapani with Roll No.: 24CHM3R02*”, submitted to the faculty of “*DEPARTMENT OF CHEMICAL ENGINEERING*”, in partial fulfilment of the requirements for the award of the degree of Master of Technology in “*Sustainable Energy Generation and Storage Technologies*” at National Institute of Technology, Warangal during the academic year 2025.

Dr. Leela Manohar Aeshala  
Associate Professor  
Department of Chemical Engineering  
NIT Warangal

## ABSTRACT

This work presents a Smart Battery Thermal and Power Management System for PV-Battery-Hydrogen Generation System for efficient, safe photovoltaic (PV) battery charging, designed for up to 60 V solar input with a 12 V energy-storage battery, capable of compensating for fast PV power fluctuations in a Hydrogen Generation System. In this paper the system uses a microcontroller-based architecture with precision sensing components (INA219 current and voltage sensor, DS18B20 temperature sensor) and a closed-loop control method to govern the charging process. The system integrates proportional–integral–derivative (PID) control in both the PV battery charging unit and the AEM electrolyzer heating stage to ensure efficient, safe, and stable operation. The PID algorithm dynamically adjusts the charging current & voltage based on solar input and battery state-of-charge, with hysteresis-based protection that disconnects the battery when unsafe conditions occur, such as over-voltage above 12.94 V or overheating above 40.5 °C, and resumes only when values fall below 12.54 V or 38 °C.

Real-time data from DS18B20 temperature sensors monitoring battery and electrolyzer cell temperatures. For the AEM electrolyzer, which must operate between 40 °C and 70 °C for optimal efficiency, a 50 W cartridge heater raises the electrolyte and cell assembly to 40 °C within 5-10 minutes under insulation. Safety mechanisms include hardware over-temperature cut-off or overheating above 70 °C and resumes only when values fall below 65 °C, preventing electrolyzer start until stable temperature is achieved. A fault detection module with a fire/smoke sensor that triggers LCD alerts, GSM (SIM900A)-based SMS notifications, and automatic system isolation during faults, allowing for quick human action. This integrated approach ensures automated cold-start capability, precise temperature regulation, efficient PV power utilization, and robust fault protection, thereby enhancing the operational efficiency of green hydrogen production and contributing to sustainable energy storage solutions for renewable applications that prioritize efficiency, safety, and resilience.

## TABLE OF CONTENTS

<b>Chapter</b>	<b>Title</b>		<b>Page No</b>	
1.	1.1	Introduction	1-4	
	1.2	History	5	
2.	Literature Survey		6-11	
3.	Experimental Requirements		12-28	
	Hardware Components:			
	3.1	Power Source and Conditioning Unit		12-14
	3.2	Power Control & Switching Components		14-18
	3.3	Micro Controller (Arduino Nano)		19
	3.4	Sensors		20-22
	3.5	Communication Module		23
	3.6	Display & User Interface		24-25
	3.7	Interfacing Components		25-26
	3.8	Thermal Actuation Unit (Cartridge Heater – 230V, 50W)		27
	3.9	Software / Firmware: Arduino IDE, Libraries		27
	3.10	AEM Electrolyzer		28
4.	Project Design & Implementation		29	
	4.1	Block Diagram of Smart Battery Thermal and Power Management System for PV-Battery-Hydrogen Generation System		29
	4.2	Equivalent Circuit Model of Smart Battery Thermal and Power Management System		30
	4.3	Equivalent Circuit Model of the Electrolyzer Control Circuit		32
	4.4	Equivalent Circuit Model of the Circuit Fault Detection and Alert System		33
5.	Results and Discussion		35-57	
	5.1	Developed Smart Battery Thermal and Power Management System for PV-Battery-Hydrogen Generation System		35
	5.2	Arduino Code for PV Battery Charging with PID Control		36-40

	5.3	Arduino Code for the Electrolyzer_control_circuit	40-43
	5.4	Arduino Code for the Circuit Fault Detection and Alert System	44-45
	5.5	All Experimental Data of Developed Smart Battery Thermal and Power Management System for PV-Battery-Hydrogen Generation System	46-52
	5.6	AEM Electrolyzer Running Characteristics (V, I and P) for 5 min	53-54
	5.7	Theoretical Calculation on Hydrogen Generated by AEM Electrolyzer Running Characteristics	55-56
	5.8	Circuit Fault Detection and Alert System through SMS	57
6.	6.1	Summary and Conclusion	58
	6.2	Future Scope	59
7.		Reference	60-61
8.		Acknowledgments	62

## LIST OF TABLES

<b>Table no.</b>	<b>Title</b>	<b>Page no.</b>
3.1	Solar Panel Specifications	12
3.2	Lithium Polymer battery Specifications	13
3.3	DC-DC Buck Converter Specifications	14
3.4	MOSFET (Q1 – IRF9540N) Specifications	15
3.5	NPN Transistor (Q2 – 2N2222) Specifications	16
3.6	Schottky Diode (D1 – 1N5822) Specifications	16
3.7	1N4007 Diode Parameters	17
3.8	5V Single-Channel Relay Module Specifications	18
3.9	Arduino Nano Specifications	19
3.10	INA219 Current Sensor Specifications	20
3.11	DS18B20 Digital temperature sensor Specifications	21
3.12	MQ-4 Smoke Sensor Specifications	22
3.13	GSM Module (SIM900A) Specifications	23
3.14	OLED Display (128x64) Specifications	24
3.15	16x2 LCD Pin Configuration	25
3.16	Electrical Parameters & Physical Construction of Cartridge Heater	27
3.17	AEM Electrolyzer Specifications	28
5.1	Experimental Data of Solar Panel and Smart Battery Thermal and Power Management System for PV-Battery-Hydrogen Generation System Input-Output Characteristics with Respect to Duty Cycles (Fixed Solar Irradiation)	48
5.2	Voltage Profile of Solar Panel and 12v (3p) Battery with respective to Time	49
5.3	Current Profile of 12v 6600mah Battery with respective to Time	50
5.4	SOC (%) Profile of 12v 3*2200mah Battery with respective to Time 5hrs	51
5.5	Voltage Response to Battery Over temperature Condition	52

## LIST OF FIGURES

<b>Figure no.</b>	<b>Title</b>	<b>Page no.</b>
1.1	Solar Panel, Battery, and AEM Electrolyser with Battery Thermal and Power Management System	1
1.2	AEM electrolyser Basic Working Principle	2
1.3	AEM electrolyser Internal Core Construction	2
1.4	PI Controller-Based Closed-Loop Control of DC-DC Converter	3
1.2.1	Block Diagram representing the System Design & Power Flow	5
3.1	24v, 60W Solar Panel	12
3.2	Lithium Polymer battery	13
3.3	DC-DC Buck Converter	14
3.4	MOSFET (Q1 – IRF9540N)	14
3.5	NPN Transistor (Q2 – 2N2222)	16
3.6	Schottky Diode (D1 – 1N5822)	16
3.7	1N4007 is a general-purpose silicon rectifier diode	17
3.8	Inductor (L1 – 330 µH)	17
3.9	Capacitor (100 µF)	18
3.10	Relay Module	18
3.11	Arduino Nano	19
3.12	INA219 Current Sensor	20
3.13	DS18B20 Digital temperature sensor	21
3.14	MQ-4 Smoke Sensor	22
3.15	GSM Module (SIM900A)	23
3.16	OLED Display (128x64)	24
3.17	16x2 LCD Display	25
3.18	Resistor	25
3.19	Jumper Wires	26
3.20	Breadboard	26
3.21	Cartridge Heater – 230V, 50W	27
3.22	AEM Electrolyzer	28
4.1	Block Diagram of Smart Battery Thermal and Power Management System for PV-Battery-Hydrogen Generation System	29
4.2	Equivalent Circuit Model of Smart Battery Thermal and Power Management System for PV-Battery	30
4.3	PWM-Based Battery Charging Algorithm with Voltage and Current Feedback	31
4.4	Electrolyzer Control Circuit	32
4.5	Equivalent Circuit Model of the Circuit Fault Detection and Alert System	34
5.1	Developed SBT&PMS for PV-Battery-Hydrogen Generation System	35

5.2	Voltage Profile of Solar Panel and Battery Over Time for 5hrs	48
5.3	Current Profile of Battery vs Time for 5hrs	49
5.4	SOC (%) Profile of 12v 2200mah Battery vs Time	50
5.5	Voltage Response to Battery Overtemperature Condition	51
5.6	Over Temperature Protection for AEM Electrolyzer	52
5.7	AEM Electrolyzer Running Characteristics for Volatage(V), Current(A), Power(W) with respective to Time(Sec)	54
5.8	SMS-Based Alert Notification for Circuit Fault Detection	57

## LIST OF ABBREVIATIONS

<b>Acronym</b>	<b>Expansion</b>
I2C	Inter-Integrated Circuit
SPI	Serial Peripheral Interface
USB	Universal Serial Bus
LIPO	Lithium Polymer Battery
LCD	Liquid Crystal Display
SMS	Short Message Service
GSM	Global System for Mobile Communications
IDE	Integrated Development Environment
SOC	State of Charge
PFET	P-channel Field-Effect Transistor
PID	Proportional-Integral-Derivative
PWM	Pulse Width Modulation
SBT&PMS	Smart Battery Thermal and Power Management System

# CHAPTER 1

## 1.1 INTRODUCTION:

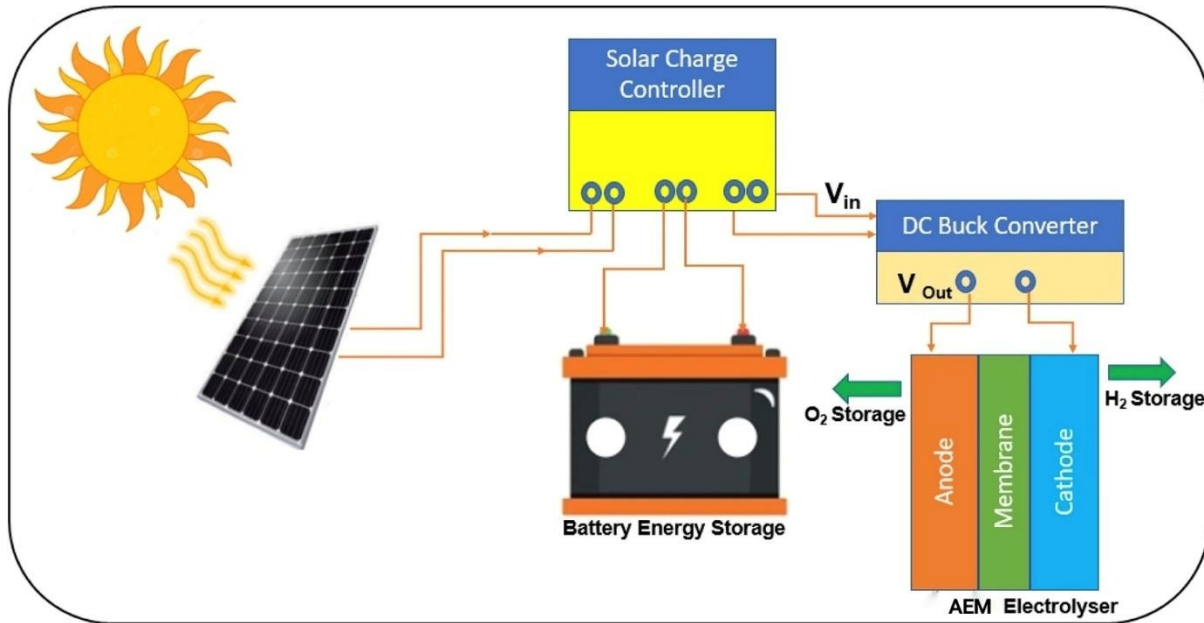


**Fig 1.1: Solar Panel, Battery, and AEM Electrolyser with Battery Thermal and Power Management System**

The increasing demand for energy, along with the simultaneous need for sustainable and eco-friendly power sources, has driven the adoption of photovoltaic (PV) systems across the globe. In regions lacking centralized electricity infrastructure, solar energy provides a clean, renewable, and cost-effective alternative to traditional fossil fuels. However, the efficiency, safety, and adaptability of solar-powered systems remain a subject of ongoing technical development. One of the most crucial components of any standalone solar system is the power controller responsible for charging the battery bank. These controllers must not only manage the energy transfer between solar panels and storage batteries but must also ensure the system operates safely under diverse environmental and electrical conditions.

The environmental protection has become widely accepted, making the transfer of clean energy urgently necessary. A potential replacement for fossil fuels is hydrogen, due to its high specific energy density and only releases water as a byproduct. However, hydrogen must be produced using a clean technique to achieve sustainability [1]. One very efficient technique is conducting water electrolysis and generating hydrogen using solar power and other renewable energy sources. It is clean, inexhaustible and noiseless. Furthermore, improvements in semiconductor technology over the past decade have led to a rise in the efficiency of solar energy panels. Also, producing hydrogen by water electrolysis is a practical and

environmentally friendly method for storing surplus power from variable renewable energy sources. Alkaline electrolyser (AEL), PEM electrolyser, solid oxide electrolyser (SOEL), and anion exchange membrane (AEM) electrolyser are the main types of electrolyzers [4,5].

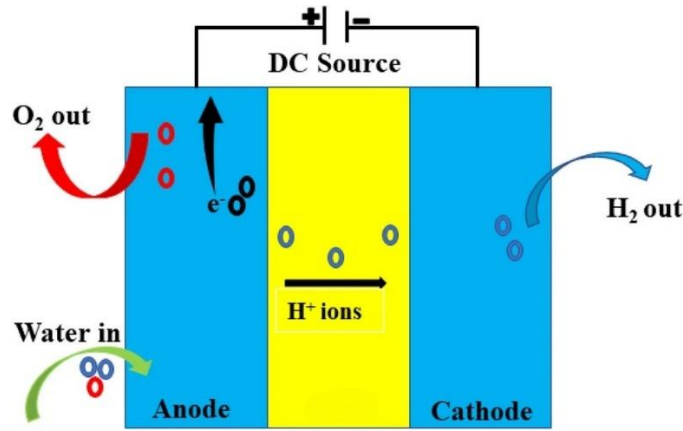


**Fig 1.2: AEM electrolyser Basic Working Principle**

The AEM electrolyser has several advantages, such as an extensive operating temperature range (40–70 °C), high current density, reduced gas permeability, enhanced energy efficiency, and ease of handling and maintenance.

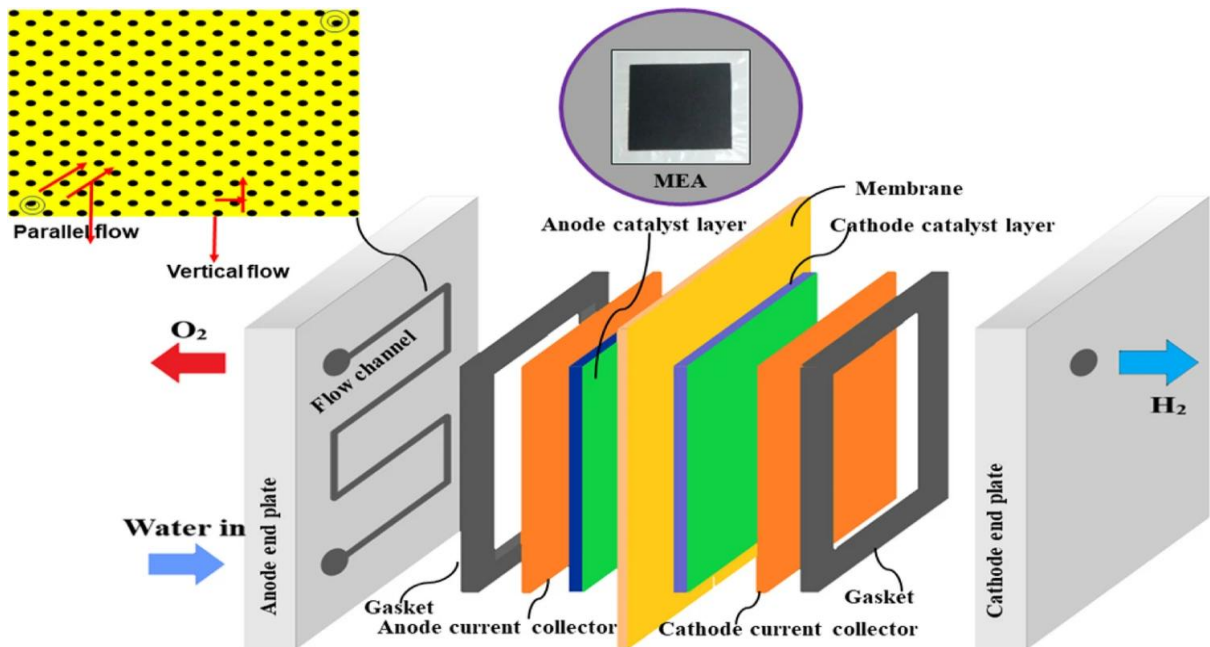


**Fig 1.3: AEM electrolyser Internal Core Construction**

However, AEM electrolyzers also have certain disadvantages, such as high specific energy consumption, lower working pressures (50 bar as compared to 200 bar for AEL), and significant investment expenses associated with employing platinum group metals, including iridium and platinum as catalyst materials. Even so, the main topic of this study is AEM electrolyser technology because of its advantages over AEL methodologies, mainly in dynamic operation.

This project focuses on the design and implementation of a smart power controller with fault detection for photovoltaic battery charging. Unlike traditional charge controllers, which often follow rigid and fixed algorithms for energy transfer, the proposed system employs real-time measurements and control logic to manage charging dynamically. At its core, the system integrates a microcontroller that receives inputs from multiple sensors including voltage, current, and temperature sensors to regulate power flow using pulse-width modulation (PWM).

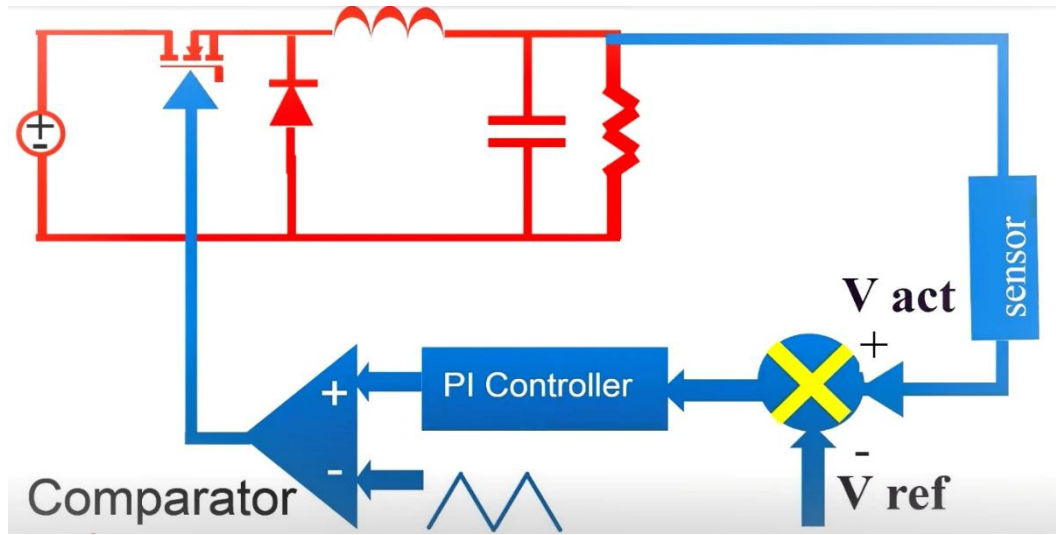


**Fig 1.4: PI Controller-Based Closed-Loop Control of DC-DC Converter**

The control strategy is based on a proportional integral derivative (PID) algorithm that adjusts the charging current depending on the difference between measured and desired values, particularly taking into account the battery's state and available solar input.

The system reads current through an INA219 high-side current sensor, enabling accurate tracking of the battery charging current. Voltage readings are obtained via analog-to-digital conversions from the battery and solar panel terminals, scaled appropriately using resistive dividers. Simultaneously, two DS18B20 temperature sensors are employed to monitor the battery's internal temperature and the ambient conditions around the controller. These readings are critical in preventing overheating and enabling the controller to take corrective actions. The software implements hysteresis-based cutoff mechanisms that disconnect the charging process if the battery temperature exceeds a predefined safe limit, resuming only after a sufficient cool-down. Similarly, over-voltage lockout is implemented, where the charging is stopped once the battery voltage crosses a safe upper threshold, and resumes only when it drops below a defined margin.

To improve battery health and extend its lifetime, the controller also incorporates logic to dynamically limit the maximum charging current based on the battery's state of charge. This is calculated by estimating the battery voltage and mapping it to a percentage scale, from a deeply discharged to a fully charged state. Lower battery levels permit higher charging currents to speed up recovery, while nearing full charge results in reduced current to prevent overcharging and stress. The actual control output—a duty cycle value ranging from 0 to 100% is applied to a power field-effect transistor (PFET), which acts as the switching element regulating the current flow to the battery.

A key aspect of the design is its user interface and data visualization capability. The system uses an OLED display to present real-time information about the charging process. Parameters such as battery current, battery voltage, solar input voltage, charge percentage, battery temperature, and ambient temperature are updated periodically. The display also uses symbols and short text indicators to convey system states—such as “CHRG” for active charging, “FULL” for voltage lockout, and “HOT” in case of temperature-based shutdown. In the event of overheating, a blinking mechanism visually alerts the user on the display, enhancing usability and awareness. These features ensure that the end user, even without technical expertise, can easily interpret the system’s operation and health.

The following are the novel contributions of the research that have been presented:

- A battery has been integrated into the green hydrogen production system to address the impact of fast fluctuation or intermittent nature of solar PV.
- This study considers the static electrical equivalent model of commercially available AEM electrolyser instead of the equivalent resistive model.
- P&O MPPT Controller for PV optimal energy harvesting, bidirectional charge controller for energy management and stabilizing the DC link voltage, and PI controller for PEM electrolyser control have been used in this study.
- Smart Battery Thermal and Power Management System that replaces the traditional Battery Management System (BMS).
- Advanced Safety technology for Circuit Fault & Fire detection.
- Overheat Protection for Battery & AEM Focusing on Safety preventing explosion & hazard detection.
- A comparative analysis has been done for systems integrated with and without batteries, and the improved efficiency and hydrogen production with the incorporation of batteries have been demonstrated.

## 1.2 History

The principle of water electrolysis was discovered in the 18th century, when Van Troostwijk and Deiman used an electrostatic generator to decompose water into hydrogen and oxygen. As early as the 19th century, scholars proposed the photovoltaic effect. With the continuous deepening of research, various research methods have emerged in the field of solar photovoltaic technology. Solar photovoltaic (PV) technology can utilize solar panels to absorb sunlight, thereby directly converting the radiant energy of sunlight into electrical energy.

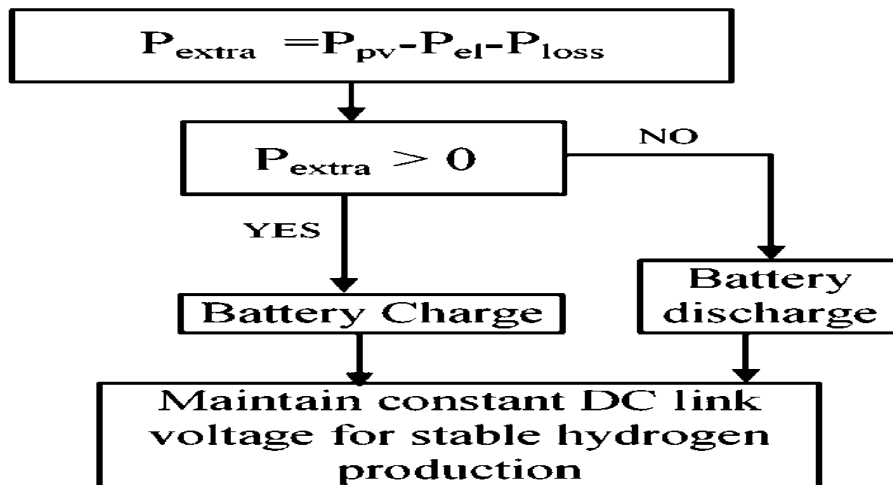


**Fig 1.2.1: Block Diagram representing the System Design & Power Flow**

In 1970, John Bockris, a South African electrochemist, proposed that hydrogen could be a fuel source from a chemical reaction between water and solar energy. In his 1975 book, Energy, the Solar Hydrogen Alternative, he explained the process and suggested using hydrogen as an energy medium. At this point, the form of current is direct current. To turn it into AC power, which is suitable for general use, you need to add equipment such as inverters. Solar photovoltaic technology is a clean energy technology that produces low environmental pollution during use and has advantages such as renewability and sustainability. Therefore, it is highly praised. Solar photovoltaic technology is suitable for various applications, such as solar photovoltaic power plants, photovoltaic agriculture, and rooftop solar photovoltaic power generation. At present, solar photovoltaic technology is mainly applied in the field of power generation, including large-scale solar power plants and distributed photovoltaic power generation. At the same time, solar photovoltaic technology is gradually being promoted in fields such as construction and transportation. summarizes the different research methods of solar photovoltaic technology and the main research conclusions obtained under different technological applications.

## CHAPTER 2

### Literature Review

A progressive body of research over the past decade has shaped the understanding and technological direction of PV-battery-electrolyzer systems, beginning with the foundational insights provided by Kikuchi et al. [3] in 2018, who established that harmonizing photovoltaic power with battery storage significantly improves the economic feasibility and operational consistency of PEM electrolyzers, particularly under off-grid conditions where solar intermittency directly disturbs the DC link stability. Their techno-economic analysis revealed that battery-assisted smoothing lowers electrolyzer oversizing requirements and reduces hydrogen cost per unit, thereby forming the earliest evidence that power buffering is essential for long-term viability.

Soon after, Xin Cai et al. [4] in 2021 expanded the conversation by demonstrating how real-world PV fluctuations accelerate PEM electrolyzer degradation—showing a voltage attenuation rate of 7.8 mV/h at 1 A/cm<sup>2</sup>, twice as high as constant-current operation, and confirming irreversible 48.3% MEA reaction-area loss even after metal-ion removal treatments. These findings validated the necessity of stable power conditioning and motivated the development of advanced sensing and protective circuitry in later works. By 2022, Fuad Alhaj Omar [7] introduced a neural-network-based Improved MPPT (IMPPT) approach that addressed mismatch losses between PV output and electrolyzer requirements, achieving 91% conversion efficiency—far surpassing conventional P&O methods—which signalled a shift from basic voltage tracking to intelligent power-electronic coordination. In parallel, power-processing challenges for large-scale electrolyzers were examined by Yodwong et al. [6] in 2020, who showed that conventional thyristor rectifiers introduce severe ripple and reactive power issues, increasing specific energy consumption; their suggestion to adopt high-frequency DC/DC stages, interleaved converters, and active-filter-based conditioning laid the groundwork for compact, low-ripple converter architectures in emerging hydrogen systems. Around the same period, Alonge et al. [8] (2020) proposed a robust H<sub>2</sub>/H<sup>∞</sup>-based controller for isolated DC/DC converters in micro-wind-powered electrolyzer setups, demonstrating superior dynamic performance over PI controllers and reinforcing the importance of mathematically grounded, disturbance-resilient control strategies for fluctuating renewable sources. As solar-powered water electrolysis entered a phase of widespread experimentation, Şahin [2] (2020) illustrated—through MATLAB/Simulink simulations—the value of coordinated MPPT and buck-converter regulation, achieving over 90% efficiency under high

irradiance while proving that voltage and current stabilization directly determine hydrogen-generation consistency. This theme was markedly strengthened by Awad et al. [1] (2023), who emphasized temperature regulation as central to PEM electrolyzer longevity, showing that every 10 °C rise above the ideal 50–80 °C range halves membrane life through accelerated degradation, ohmic loss, catalyst corrosion, and non-uniform current distribution; their recommendations for advanced cooling, PCM integration, and thermally reinforced membrane materials became the scientific backbone for multi-sensor thermal monitoring in modern systems. In 2024, Kumar and Samuel [5] demonstrated that hydrogen generation improves by nearly 10% when a battery-buffered PV system is paired with PI-controlled DC-link stabilization, proving experimentally that mitigating fast PV fluctuations yields longer electrolyzer lifespan and smoother operational cycles. Complementing the control-side innovations, Al-Mut et al. [9] (2023) addressed partial shading and tracking inaccuracies in PV arrays through a hybrid PSO–PID MPPT method, improving convergence speed and reducing tracking errors under dynamic environmental conditions; however, unlike their optimization-centric approach, modern systems increasingly incorporate safety-critical protections—temperature, smoke, over-voltage, current limiting—reflecting a transition from purely efficiency-driven designs to reliability-oriented architectures. Most recently, Taghezouit et al. [10] (2024) highlighted the rise of model-based and machine-learning-assisted diagnostics ranging from one-diode PV models to SVR and PCA-based anomaly detection showing that accurate digital twins and predictive algorithms are now indispensable for fault detection, system modelling, and performance forecasting. Collectively, these ten studies show a chronological evolution: initial cost and feasibility studies led to deeper understanding of degradation mechanisms, followed by intelligent MPPT advancements, converter-control innovations, battery-buffered stabilization strategies, and finally modern sensing, modelling, and predictive-protection frameworks that now define the next generation of PV-battery-hydrogen energy systems.

The progression of PV-Battery-Electrolyzer research has consistently emphasized the importance of maintaining thermal stability, electrical smoothness, and predictive control to guarantee safe and efficient hydrogen production. Early insights established that AEM/PEM electrolyzers must operate within specific thermal windows to avoid membrane and catalyst degradation, reinforcing that temperature management is not an auxiliary feature but a central requirement for long-term stack durability. As renewable systems matured, researchers demonstrated that fluctuating PV power not only reduces hydrogen output but significantly increases operational stress, making dynamic power conditioning essential. MPPT-controlled

DC–DC stages proved crucial in shaping PV input to match the electrolyzer’s inherently low-voltage, high-current demand, while battery buffering became a necessary evolution to smooth sharp irradiance-driven transients that otherwise cause internal ohmic heating, catalyst peeling, and accelerated electrochemical decay. Real-world degradation studies using SEM validation confirmed that the harmful effects of PV variability are measurable and irreversible, reinforcing the need for hybrid PV–Battery–Electrolyzer architectures capable of stabilizing both thermal and electrical domains. As system integration advanced, PI-regulated battery-supported topologies demonstrated measurable increases in overall efficiency and lifespan by minimizing ripple and keeping the electrolyzer within its optimal operating band, directly mitigating the degradation pathways previously identified. Complementary power-electronic developments highlighted that traditional rectifiers introduce problematic current ripple, whereas modern high-frequency converters and interleaved DC chopper stages provide cleaner, ripple-minimized DC crucial for membrane protection. To further improve energy capture under complex irradiance conditions such as partial shading, intelligent MPPT algorithms based on neural estimators and hybrid PSO–PID structures emerged, ensuring continuous operation at the true maximum power point. Meanwhile, predictive control frameworks such as H<sub>2</sub>/H<sub>∞</sub>-based strategies established a more robust foundation for maintaining converter stability under renewable variability, offering superior ripple suppression compared to conventional PI regulators. The reliability dimension expanded further with model-based fault-detection methodologies that diagnose PV disturbances before they reach the battery or electrolyzer, inspiring the integration of real-time monitoring, predictive alerts, and automated protection in modern systems. These insights collectively shaped the development of advanced architectures—such as the Smart Battery Thermal and Power Management System with GSM-based fault notifications, over-temperature shutdown at 70 °C with auto-resume at 65 °C, fire/smoke-triggered isolation, hysteresis-based voltage protection, PID-regulated heating for AEM electrolyzers, and stabilized PV-battery interfacing—all converging into a unified, intelligent, safe, and resilient platform designed to overcome every operational challenge identified across the entire research timeline.

The evolution of hydrogen production systems powered by renewable energy has increasingly highlighted the necessity of thermal stability, power regulation, and electrolyzer protection, forming a consistent theme across multiple research efforts. Early studies such as Awad et al. [1] established a fundamental understanding that PEM/AEM electrolyzers must maintain operation within an optimal band—typically 50–80 °C—to preserve membrane integrity, prevent catalyst degradation, and ensure long-term hydrogen yield. Their insights laid the

groundwork for recognizing temperature as the cornerstone of sustainable electrolyzer operation. They showed that even a 10 °C increase above the limit can halve electrolyzer lifespan, forcing designers to incorporate intelligent cooling, membrane reinforcement, and adaptive thermal control strategies in newer systems.

As renewable energy-powered hydrogen systems matured, the next area of focus became PV-to-electrolyzer energy matching, explored in depth by Sahin [2]. His demonstration of MPPT-controlled DC-DC regulation showed that hydrogen production efficiency dramatically improves when the fluctuating PV voltage is conditioned through a buck converter and PI control. The study's MATLAB simulations proved that real-time power shaping is indispensable, especially as electrolyzers demand high current at low voltage, making direct PV coupling inefficient. This research directly aligned with the emerging understanding that maintaining stable electrolyzer temperature is not enough—the electrical power input must also be dynamically shaped to prevent stress conditions that accelerate thermal and electrochemical degradation highlighted in [1].

Studies such as Kikuchi et al. [3] pushed the discussion further by bringing battery storage into the conversation. Their techno-economic analysis demonstrated that PV intermittency not only reduces hydrogen output but also increases operational cost, as frequent voltage fluctuations force electrolyzers to operate inefficiently. By integrating batteries to smooth DC-link variations, they showed that electrolyzers can operate closer to their rated point, markedly reducing power oscillations that otherwise increase ohmic losses and local temperature spikes—effects already cautioned by Awad et al. Their work demonstrated that PV–Battery–Electrolyzer hybridization is not merely an economic choice but a technical requirement for long-term system durability.

The need for deeper degradation analysis under real-world PV fluctuations was addressed by Xin Cai et al. [4], who revealed how direct PV variability induces severe catalyst peeling, doubling the voltage attenuation rate compared to steady-state operation. SEM imaging confirmed permanent MEA damage, validating earlier warnings that fluctuating thermal and electrical stresses accelerate degradation. Their Markov-based fluctuation modelling connected perfectly with the earlier MPPT and battery-assisted work by showing that electrochemical decay is not theoretical—it is measurable and irreversible. This strengthened the argument for control-oriented architectures that combine MPPT, energy storage, and thermal buffering.

The next major advancement came from Kumar and Samuel [5], who developed a modern architecture using an MPPT–Battery–Electrolyzer integration with PI-based voltage regulation. Their findings reinforced that battery-assisted stabilization yields 10% higher system efficiency, reduces electrolyzer voltage ripple, and extends lifespan—directly addressing MEA degradation described in [4]. Their intelligent control approach created a bridge between earlier PV regulation methods [2], battery-leveling strategies [3], and the electrochemical degradation insights of [1] and [4], offering a unified operational solution. Parallel to these innovations, power-electronic research by Yodwong et al. [6] highlighted the critical role of AC–DC converters and ripple suppression. They demonstrated that thyristor-based rectifiers—though widely used—introduce heavy current ripple, increasing specific energy consumption and damaging electrolyzer components.

Their recommendation of high-frequency switching converters and interleaved DC-choppers aligned naturally with the MPPT-based power conditioning strategies in [2] and the robust converter designs required to prevent fluctuating MEA stress as noted in [4]. Collectively, these works formed an engineering consensus: clean, filtered, ripple-minimized DC is the backbone of hydrogen system longevity.

Addressing the limitations of traditional MPPT approaches, Alhaj Omar [7] proposed an IMPPT technique using a neural estimator and variable step-size control, achieving 91% efficiency, far surpassing conventional P&O (67%) and direct coupling (45%). This advancement demonstrated that modern hydrogen systems must shift from simple perturb-based control to AI-assisted dynamic optimization, particularly under complex irradiance patterns such as partial shading, high ramp-rate fluctuations, and seasonal variability. This advanced MPPT philosophy supports the battery-buffered strategies in [3] and [5] while mitigating the degradation mechanisms revealed in [4].

Further strengthening the control dimension, Alonge et al. [8] introduced a robust  $H_2/H_\infty$  control structure for DC–DC converters in micro-wind-powered electrolyzer systems. Their controller significantly reduced voltage and current ripple, outperforming classical PI regulators. This resonated directly with the need to suppress the electrochemical stress mechanisms highlighted in [1] and [4] and matched the system-wide effort to maintain stable electrolyzer conditions, regardless of renewable source variability—be it solar or wind.

Meanwhile, studies on PV system optimization under complex shading conditions, such as Al-Mut et al. [9], proposed hybrid PSO–PID controllers, ensuring global MPP detection even under partial shading. While their research focused on PV optimization, its principles extend seamlessly to hydrogen systems: maintaining maximum power extraction reduces the thermal and voltage stress transmitted to the electrolyzer, thus supporting the degradation insights from [1] and [4] and the MPPT-battery frameworks of [3], [5], and [7].

Finally, Taghezouit et al. [10] expanded the reliability perspective by demonstrating how model-based fault detection—using both parametric and data-driven methods—can diagnose PV abnormalities before they propagate into downstream systems. Inspired by this, modern PV–Battery–Electrolyzer architectures now integrate fault detection layers that combine electrical modelling, sensor data, and predictive analytics. In our system, these ideas translate into a practical safety layer: hardware over-temperature cut-off above 70 °C, auto-resume only at 65 °C, GSM (SIM900A) SMS fault notification, fire/smoke-triggered shutdown, LCD fault alerts, and full system isolation during critical events. This real-world implementation represents the natural convergence of thermal regulation [1], power stabilization [2–8], optimization [9], and predictive diagnostics [10], forming a cohesive, intelligent, and safe hydrogen production ecosystem.

# CHAPTER 3

## EXPERIMENTAL REQUIREMENTS

To design and implement a Smart Battery Thermal and Power Management System for Battery integrated with a photovoltaic (PV) power source, the following experimental requirements are necessary:

### **Hardware Components:**

#### **3.1 Power Source Unit:**

##### **a) Solar Panel / Solar Cells:**

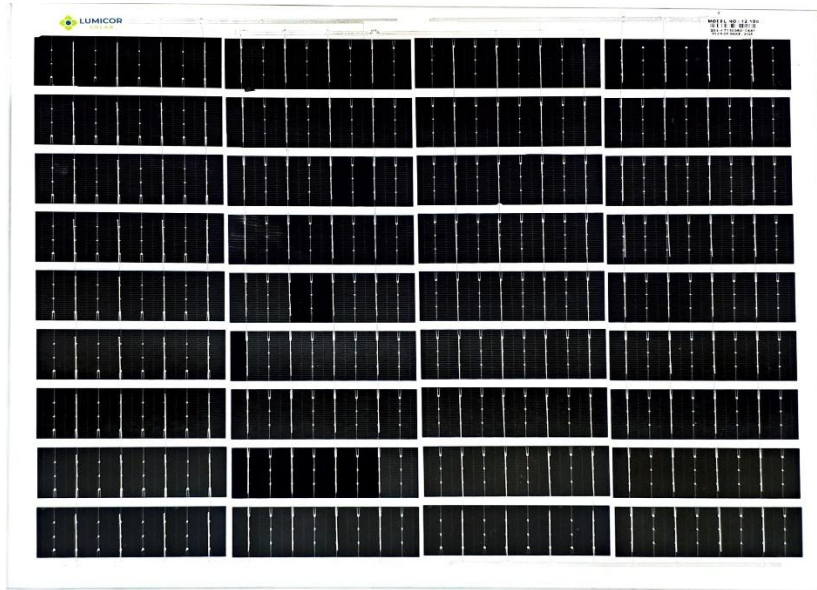


**Fig 3.1: 24v , 60W Solar Panel**

Acts as the primary renewable energy input for charging the battery.

**Table 3.1 Solar Panel Specifications**

<b>Component</b>	<b>Sub-component</b>	<b>Specification</b>
Power generating unit	Solar PV Module	
	Number of modules	2
	Type	Mono-crystalline
	Pmax (Maximum Power)	60 W
	Voc (Open Circuit Voltage)	24.48 V
	Isc (Short Circuit Current)	2.45 A
	Vpm (Max Peak Voltage)	20.88 V
	Ipm (Max Peak Current)	1.95 A
	FF (Fill Factor)	0.70
	Eff. module	13.95 %
	Eff. cell	15.8 %

**b) Battery Storage:** 12V, 2200mAh Lithium Polymer battery.

The output of solar PV is unpredictable due to temporal and environmental conditions. A battery energy storage system was incorporated to solve this problem, maintain the DC bus voltage, diminish output power fluctuations.



**Fig 3.2: Lithium Polymer battery**

**Table 3.2 Lithium Polymer battery Specifications**

Component	Sub-component	Specification
Battery	Type	LiPo (Lithium Polymer)
	Brand	Wild Scorpion
	Model	NANO
	Capacity	2200mAh
	Voltage	11.1V
	Discharge Rate (C-rating)	30C
	Voltage per cell	3.7V
	Configuration	XT60 Connector

c) DC-DC Buck Converter:

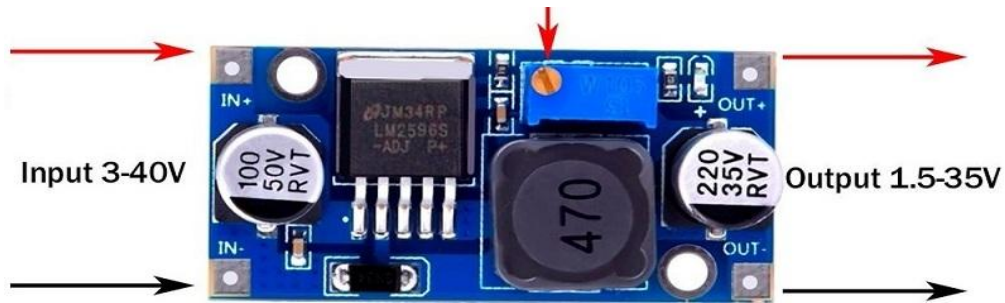


Fig 3.3: DC-DC Buck Converter

Table 3.3 DC-DC Buck Converter Specifications

Component	Sub-component	Specification
Power conversion unit	DC-DC Buck Converter Module	LM2596
Input voltage		3 V to 40 V
Output voltage	Adjustable	1.5 V to 35 V
Output current	Rated	2 A
Output current (max)	With additional heatsink	3 A
Efficiency	Typical	Up to 92%
Switching frequency	Fixed	~150 kHz
Voltage regulation	Line and load regulation	±1% (typical)
Ripple and noise	Output voltage ripple	<30mV (typical, depends on load)
Module size		~43 mm × 21 mm × 14 mm

### 3.2 Power Control & Switching Components:

a) MOSFET (Q1 – IRF9540N) :

P-Channel MOSFET used for high-side switching to control power from the solar panel.

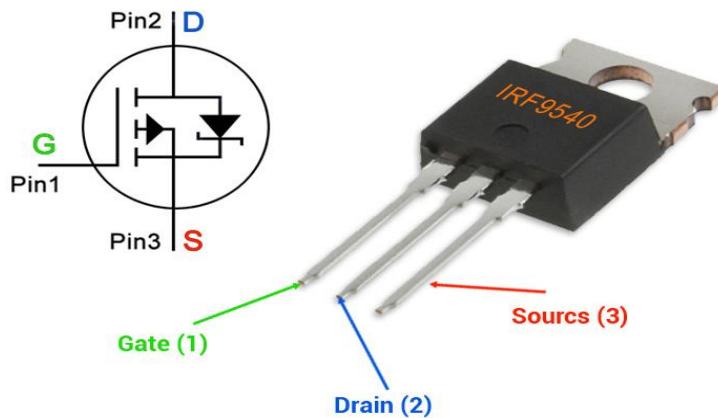


Fig 3.4: MOSFET (Q1 – IRF9540N)

**Table 3.4 MOSFET (Q1 – IRF9540N) Specifications**

<b>SPECIFICATIONS</b> ( $T_J = 25^\circ\text{C}$ , unless otherwise noted)						
PARAMETER	SYMBOL	TEST CONDITIONS	MIN.	TYP.	MAX.	UNIT
<b>Static</b>						
Drain-source breakdown voltage	$V_{DS}$	$V_{GS} = 0 \text{ V}, I_D = -250 \mu\text{A}$	-100	-	-	V
$V_{DS}$ temperature coefficient	$\Delta V_{DS}/T_J$	Reference to $25^\circ\text{C}$ , $I_D = -1 \text{ mA}$	-	-0.087	-	$\text{V}/^\circ\text{C}$
Gate-source threshold voltage	$V_{GS(\text{th})}$	$V_{DS} = V_{GS}, I_D = -250 \mu\text{A}$	-2.0	-	-4.0	V
Gate-source leakage	$I_{GSS}$	$V_{GS} = \pm 20 \text{ V}$	-	-	$\pm 100$	$\text{nA}$
Zero gate voltage drain current	$I_{DSS}$	$V_{DS} = -100 \text{ V}, V_{GS} = 0 \text{ V}$	-	-	-100	$\mu\text{A}$
		$V_{DS} = -80 \text{ V}, V_{GS} = 0 \text{ V}, T_J = 150^\circ\text{C}$	-	-	-500	
Drain-source on-state resistance	$R_{DS(\text{on})}$	$V_{GS} = -10 \text{ V}$	$I_D = -11 \text{ A}^b$	-	-	0.20
Forward transconductance	$g_{fs}$	$V_{DS} = -50 \text{ V}, I_D = -11 \text{ A}^b$	6.2	-	-	S
<b>Dynamic</b>						
Input capacitance	$C_{iss}$	$V_{GS} = 0 \text{ V},$ $V_{DS} = -25 \text{ V},$ $f = 1.0 \text{ MHz, see fig. 5}$	-	1400	-	$\text{pF}$
Output capacitance	$C_{oss}$		-	590	-	
Reverse transfer capacitance	$C_{rss}$		-	140	-	
Total gate charge	$Q_g$	$V_{GS} = -10 \text{ V}$	$I_D = -19 \text{ A}, V_{DS} = -80 \text{ V},$ see fig. 6 and 13 <sup>b</sup>	-	-	61
Gate-source charge	$Q_{gs}$			-	-	14
Gate-drain charge	$Q_{gd}$			-	-	29
Turn-on delay time	$t_{d(\text{on})}$	$V_{DD} = -50 \text{ V}, I_D = -19 \text{ A},$ $R_g = 9.1 \Omega, R_D = 2.4 \Omega, \text{ see fig. 10}^b$	-	16	-	$\text{ns}$
Rise time	$t_r$		-	73	-	
Turn-off delay time	$t_{d(\text{off})}$		-	34	-	
Fall time	$t_f$		-	57	-	
Gate input resistance	$R_g$	$f = 1 \text{ MHz, open drain}$		0.3	-	1.6
Internal drain inductance	$L_D$	Between lead, 6 mm (0.25") from package and center of die contact		-	4.5	-
Internal source inductance	$L_S$			-	7.5	-
<b>Drain-Source Body Diode Characteristics</b>						
Continuous source-drain diode current	$I_S$	MOSFET symbol showing the integral reverse p-n junction diode		-	-	-19
Pulsed diode forward current <sup>a</sup>	$I_{SM}$			-	-	-72
Body diode voltage	$V_{SD}$	$T_J = 25^\circ\text{C}, I_S = -19 \text{ A}, V_{GS} = 0 \text{ V}^b$	-	-	-5.0	V
Body diode reverse recovery time	$t_{rr}$	$T_J = 25^\circ\text{C}, I_F = -19 \text{ A}, dI/dt = 100 \text{ A}/\mu\text{s}^b$	-	130	260	ns
Body diode reverse recovery charge	$Q_{rr}$		-	0.35	0.70	$\mu\text{C}$
Forward turn-on time	$t_{on}$	Intrinsic turn-on time is negligible (turn-on is dominated by $L_S$ and $L_D$ )				

**b) NPN Transistor (Q2 – 2N2222) :**

Used to control the gate of the MOSFET (gate driver logic using Arduino PWM).

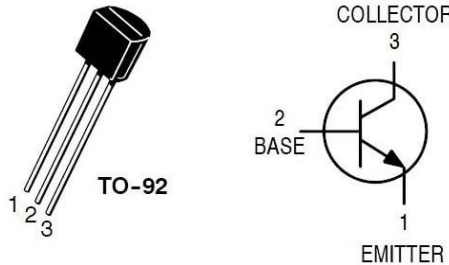


**Fig 3.5: NPN Transistor (Q2 – 2N2222)**

**Table 3.5: NPN Transistor (Q2 – 2N2222) Specifications**

Characteristic	Symbol	Value	Unit
Collector – Emitter Voltage	$V_{CEO}$	40	Vdc
Collector – Base Voltage	$V_{CBO}$	75	Vdc
Emitter – Base Voltage	$V_{EBO}$	6.0	Vdc
Collector Current – Continuous	$I_C$	600	mAdc
Total Device Dissipation @ $T_A = 25^\circ\text{C}$ Derate above $25^\circ\text{C}$	$P_D$	625 5.0	mW mW/ $^\circ\text{C}$
Total Device Dissipation @ $T_C = 25^\circ\text{C}$ Derate above $25^\circ\text{C}$	$P_D$	1.5 12	W mW/ $^\circ\text{C}$
Operating and Storage Junction Temperature Range	$T_J, T_{stg}$	-55 to +150	$^\circ\text{C}$

**c) Schottky Diode (D1 – 1N5822) :**

Prevents backflow of current from battery to solar panel.

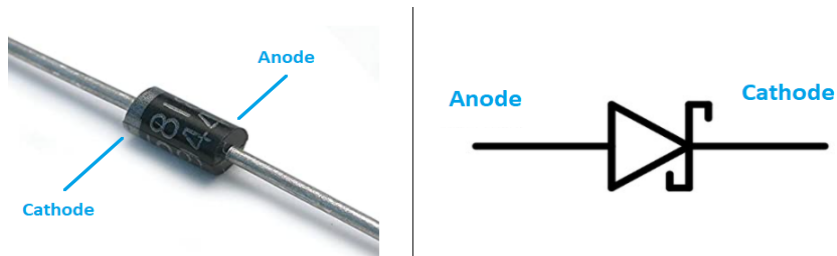


**Fig 3.6: Schottky Diode (D1 – 1N5822)**

**Table 3.6: Schottky Diode (D1 – 1N5822) Specifications**

$I_F(AV)$	3.0 A
$V_{RRM}$	20 V, 30 V, 40 V
$I_{FSM}$	80 A
$V_F$	0.475 V, 0.500 V, 0.525 V
$T_J$ max.	125 $^\circ\text{C}$
Package	DO-201AD
Diode variations	Single

**d) 1N4007 Diode (D1) :**

The 1N4007 is a general-purpose silicon rectifier diode placed at the solar panel input to provide reverse polarity protection, preventing damage to the smart power controller and other downstream components in case the panel is connected with reversed terminals.

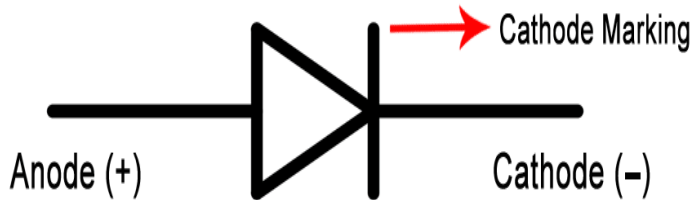


**Fig 3.7: 1N4007 Diode**

**Table 3.7: 1N4007 Diode Parameters**

Parameter	Value / Description
Maximum Repetitive Peak Reverse Voltage (VRRM)	1000 V
Average Forward Current (IF(AV))	1 A
Peak Forward Surge Current (IFSM)	30 A (for 1 cycle)
Maximum Forward Voltage (VF)	1 V at 1 A
Maximum Reverse Current (IR)	5 $\mu$ A at rated voltage
Typical Junction Capacitance (Cj)	15 pF
Operating Temperature Range	-55°C to +150°C
Package	DO-41 (through-hole)

**e) Inductor (L1 – 330  $\mu$ H) :**

Part of the buck converter circuit for current smoothing.



**Fig 3.8: Inductor (L1 – 330  $\mu$ H)**

**f) Capacitors (C1, C2 – 100  $\mu$ F, 25V) :**

For input/output filtering in the buck converter.

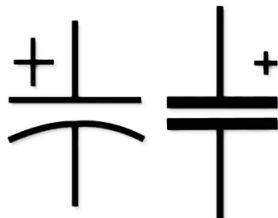


**Fig 3.9: Capacitor (100  $\mu$ F, 25V)**

**g) 5V Single-Channel Relay Module :**

Relay is an electromechanical device that uses an electric current to open or close the contacts of a switch. The single-channel relay module is much more than just a plain relay, it comprises of components that make switching and connection easier and act as indicators to show if the module is powered and if the relay is active or not.

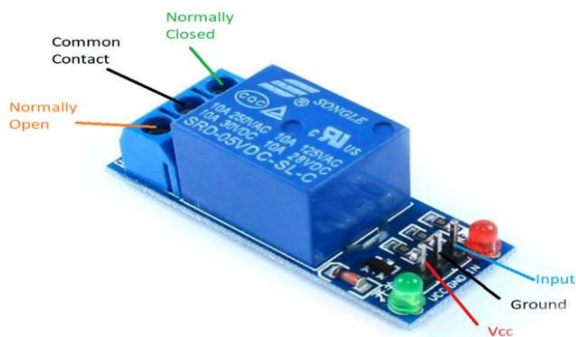


**Fig 3.10: Relay Module**

**Table 3.8: 1N4007 Diode Parameters**

Parameter	Value / Description
Supply voltage	3.75V to 6V
Quiescent current	2mA
Current when the relay is active	~70mA
Relay maximum contact voltage	50VAC or 30VDC
Relay maximum current	10A

### 3.3 Micro Controller (Arduino Nano):

**Arduino Nano** is an 8-bit microcontroller, specifically Central controller that manages sensor data acquisition, PWM control, data logging, and display logic.

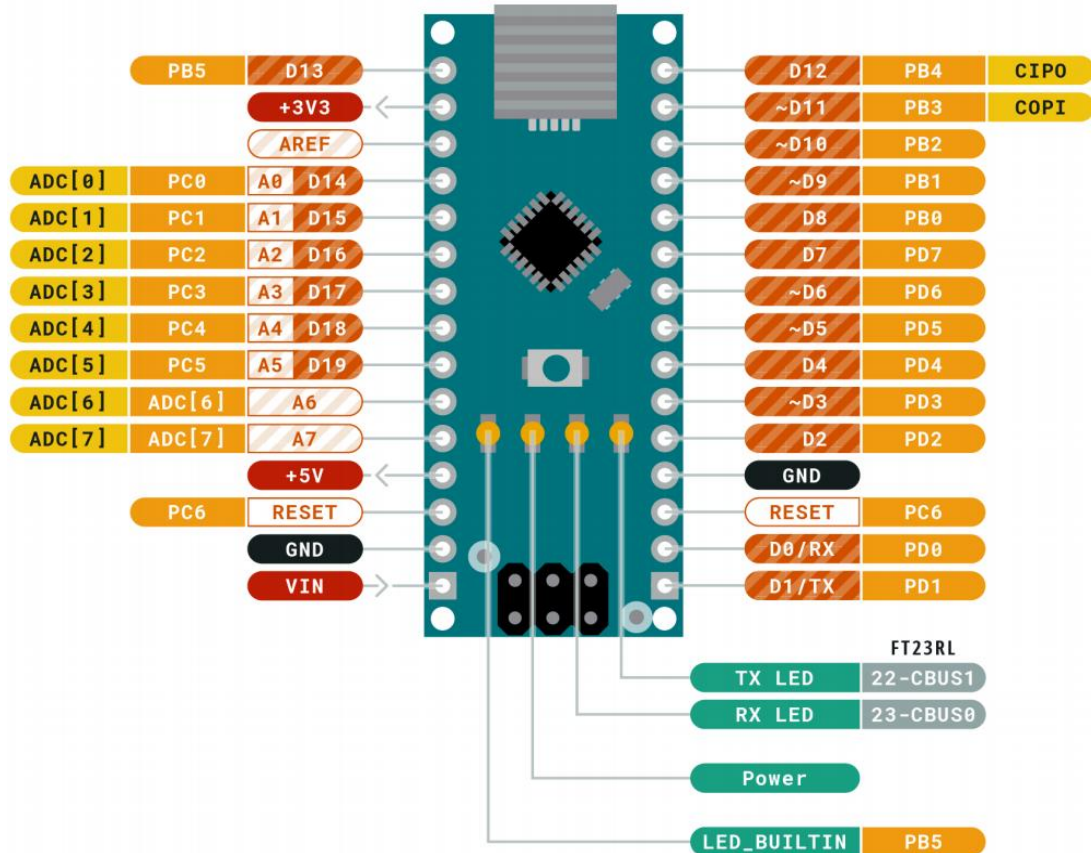


Fig 3.11: Arduino Nano

Table 3.9: Arduino Nano Specifications

Component	Sub-component	Specification
Microcontroller Unit	Microcontroller	ATmega328
	Operating Voltage	5V
	Input Voltage (recommended)	7 – 12V
	Input Voltage (limits)	6 – 20V
	Digital I/O Pins	14 (6 with PWM output)
	Analog Input Pins	6
	DC Current per I/O Pin	40 mA
	DC Current for 3.3V Pin	50 mA
	Flash Memory	32 KB (0.5 KB used by bootloader)
	Clock Speed	16 MHz

### 3.4 Sensors:

- **INA219:**

Precision current and voltage sensor for monitoring battery voltage, current, and power in the charging path.

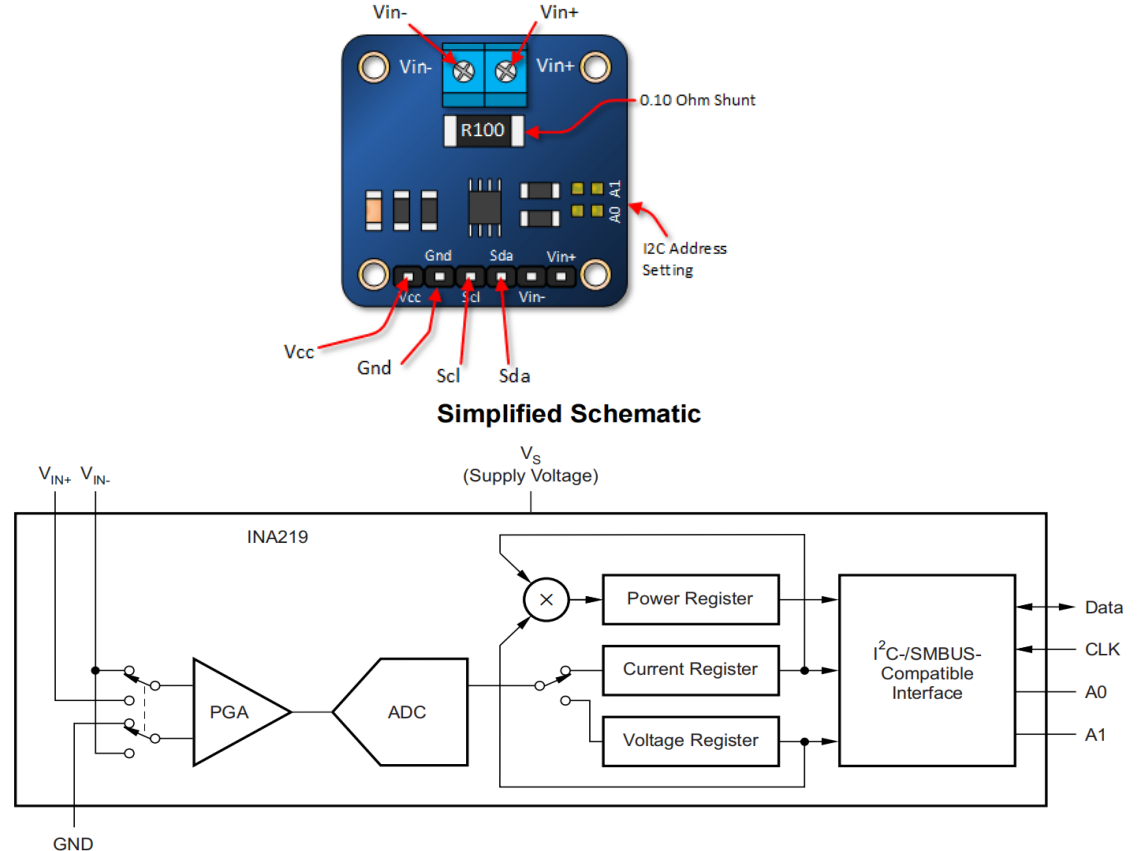


**Fig 3.12: INA219 Current Sensor**

**Table 3.10: INA219 Current Sensor Specifications**

Component	Sub-component	Specification
Voltage Range	Bus Voltage	0 to 26V
Current Range	-	$\pm 3.2A$ (with $\pm 0.8mA$ resolution)
Power Supply	-	3.0V to 5.5V
Interface	Communication	I2C or SMBus
Accuracy	Measurement Error	Max error 0.5% over entire temperature range (B grade)
Filtering	Conversion/Filtering	Programmable conversion times and filtering options available
Calibration	-	Programmable calibration registers for current/power readout

- **DS18B20:**

Digital temperature sensors for thermal monitoring, possibly used on battery and ambient conditions.



**Fig 3.13: DS18B20 Digital temperature sensor**

**Table 3.11: DS18B20 Digital temperature sensor Specifications**

Component	Sub-component	Specification
Communication	Interface	1-Wire (requires only one port pin)
Topology	Multidrop Capability	Supports multiple sensors on a single bus
Circuit Requirement	External Components	None required
Power Supply	Voltage Range	3.0V to 5.5V
Power Consumption	Standby Power	Zero standby power
Temperature Range	Measurement Range	-55°C to +125°C (or -67°F to +257°F)
Accuracy	Typical Accuracy	±0.5°C from -10°C to +85°C
Resolution	Programmable	9 to 12 bits
Conversion Time	12-bit Conversion	750 ms (max)
Alarm Feature	Alarm Settings	User-definable, nonvolatile temperature alarms
Device Identification	Alarm Search Command	Identifies devices outside programmed temperature limits
Applications	-	Thermostatic controls, industrial/consumer systems, thermometers, etc.

- **MQ-4 Smoke Sensor:**

Used to detect burnt gas (e.g., methane or LPG) as a safety measure.



**Fig 3.14: MQ-4 Smoke Sensor**

**Table 3.12: MQ-4 Smoke Sensor Specifications**

Model			MQ-4
Sensor Type			Semiconductor
Standard Encapsulation			Bakelite, Metal cap
Target Gas			Methane
Detection range			300~10000ppm(CH <sub>4</sub> )
Standard Circuit Conditions	Loop Voltage	V <sub>c</sub>	≤24V DC
	Heater Voltage	V <sub>H</sub>	5.0V±0.1V AC or DC
	Load Resistance	R <sub>L</sub>	Adjustable
Sensor character under standard test conditions	Heater Resistance	R <sub>H</sub>	26Ω±3Ω(room temp.)
	Heater consumption	P <sub>H</sub>	≤950mW
	Sensitivity	S	R <sub>s</sub> (in air)/R <sub>s</sub> (in 5000ppmCH <sub>4</sub> )≥5
	Output Voltage	V <sub>s</sub>	2.5V~4.0V (in 5000ppm CH <sub>4</sub> )
	Concentration Slope	α	≤0.6(R <sub>5000ppm</sub> /R <sub>1000ppm</sub> CH <sub>4</sub> )
Standard test conditions	Temp. Humidity		20°C±2°C; 55%±5%RH
	Standard test circuit		V <sub>c</sub> :5.0V±0.1V V <sub>H</sub> :5.0V±0.1V
	Preheat time		Not less than 48 hours
	O <sub>2</sub> content		21% (not less than 18%) O <sub>2</sub> concentration effects initial value, sensitivity and repeatability.

### 3.5 Communication Modules:

- **GSM Module (SIM900A):**

Used to send alerts (SMS) in case of fault conditions detected by sensors.

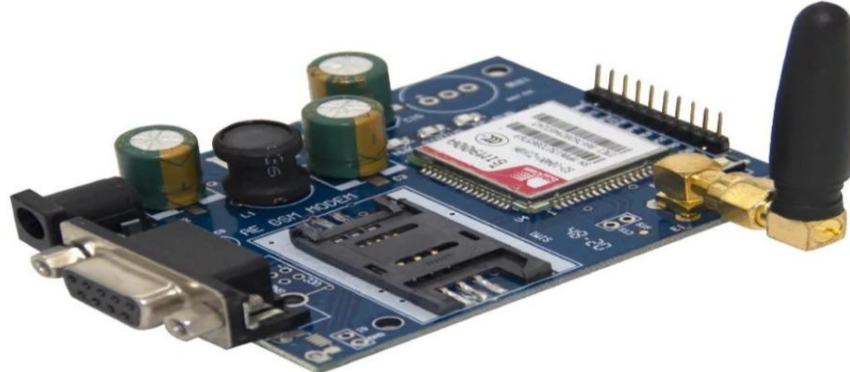


**Fig 3.15: GSM Module (SIM900A)**

**Table 3.13: GSM Module (SIM900A) Specifications**

Component	Sub-component	Specification
Power Supply	Voltage Range	3.4V – 4.5V
Power Saving Mode	Sleep Mode Current	1.5 mA
Frequency Bands	Supported Bands	EGSM900, DCS1800 (Dual-band)
	Band Selection	Auto or AT command configurable
GSM Class	-	Small MS
GPRS Connectivity	Multi-slot Support	Class 10 (default), Class 8 (optional)
Transmitting Power	EGSM 900	Class 4 (2W)
	DCS 1800	Class 1 (1W)
Operating Temperature	-	-30°C to +80°C
Data Transfer (GPRS)	Download	Max 85.6 KBps
	Upload	Max 42.8 KBps
Supported Services	-	CSD, USSD, SMS, FAX
Interfaces	Keypad Interface	Yes
	Display Interface	Yes
	Real Time Clock	Yes
	UART Interface	Supported
SIM Card	-	Single SIM supported
Firmware	Upgrade	Via debug port
Communication	-	Using AT commands

### 3.6 Display & User Interface:

- **OLED Display (128x64):**

Used with the Arduino Nano to display voltage, current, Battery temperature, Solar Ambient temperature and Charging Status.



**Fig 3.16: OLED Display (128x64)**

**Table 3.14: OLED Display (128x64) Specifications**

Component	Sub-component	Specification
Pin	VCC (Power Supply)	Supply 3.3V / 5V
	SDA / MOSI	Serial Clock For I <sup>2</sup> C or SPI
	SDA / MOSI	Serial Data For I <sup>2</sup> C or SPI
	RES	Reset Present in some modules (optional)
	DC / D/C	Data/Command Control SPI only (optional)
I2C Address	-	Typically 0x3C (may vary)
Display Controller	Driver IC	SSD1306
Resolution	-	128 × 64 pixels
Interface	Communication	I <sup>2</sup> C (default) or SPI
Viewing Angle	Alarm Settings	>160°
Pixel Colour	-	Monochrome (white / blue / yellow depending on model)
Operating Temperature	-	-30°C to +70°C
Module Dimensions	-	~27 mm × 27 mm × 4.1 mm
Compatibility	-	Fully compatible, widely supported by libraries
SPI Mode (if used)	-	9-bit format, 1st bit = Data/Command

- **16x2 LCD Display:**

Connected to the Arduino Nano for local monitoring (especially fault alert).

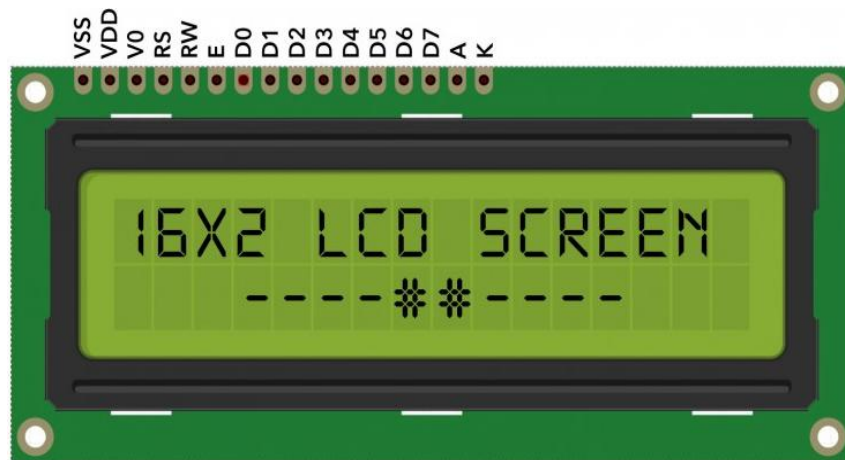


**Fig 3.17: 16x2 LCD Display**

**Table 3.15: 16x2 LCD Pin Configuration**

No	Symbol	Function
1	VSS	Ground
2	VDD	5V + (Power Supply)
3	V0	Contrast Adjustment
4	RS	Register Select
5	RW	Read/Write
6	E	Enable
7	D0 – D7	Data Buses
8	A	Anode (5V+)
9	K	Cathode (GND)

### 3.7 Interfacing Components

#### Resistors:

- Pull-up resistors for DS18B20 sensors ( $4.7\text{k}\Omega$ ).
- Voltage dividers for INA219 interfacing.
- Base resistor for 2N2222 transistor ( $2\text{k}\Omega$ ).



**Fig 3.18: Resistor**

**Jumper Wires & Breadboards:** For connections and prototyping.

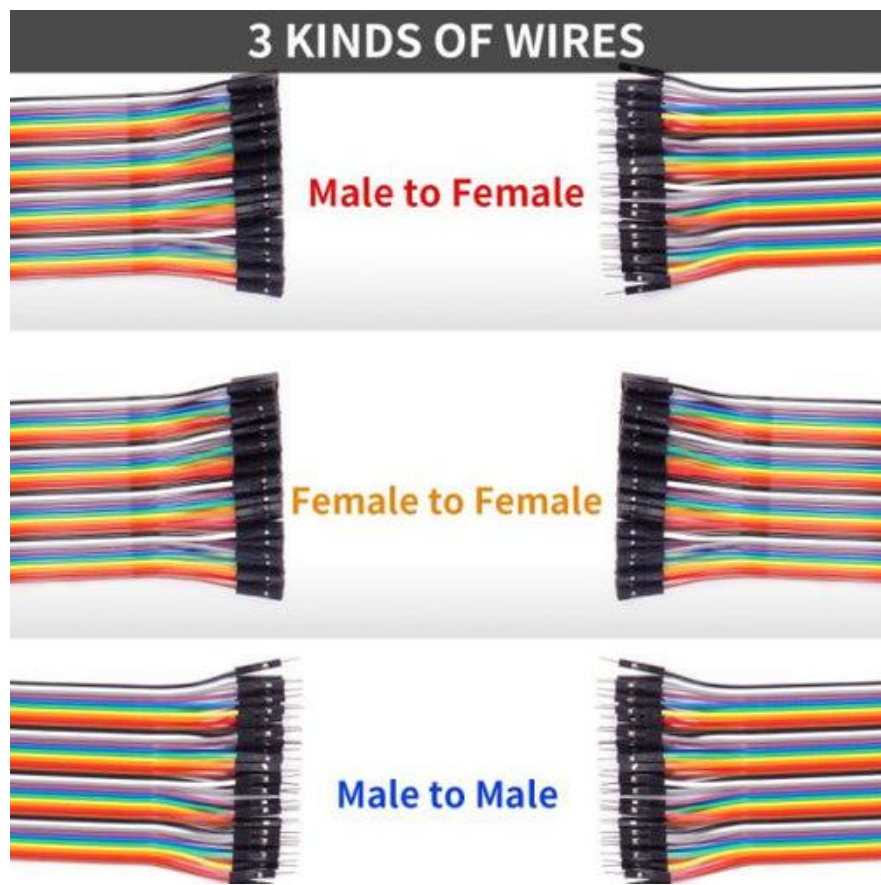


**Fig 3.19: Jumper Wires**

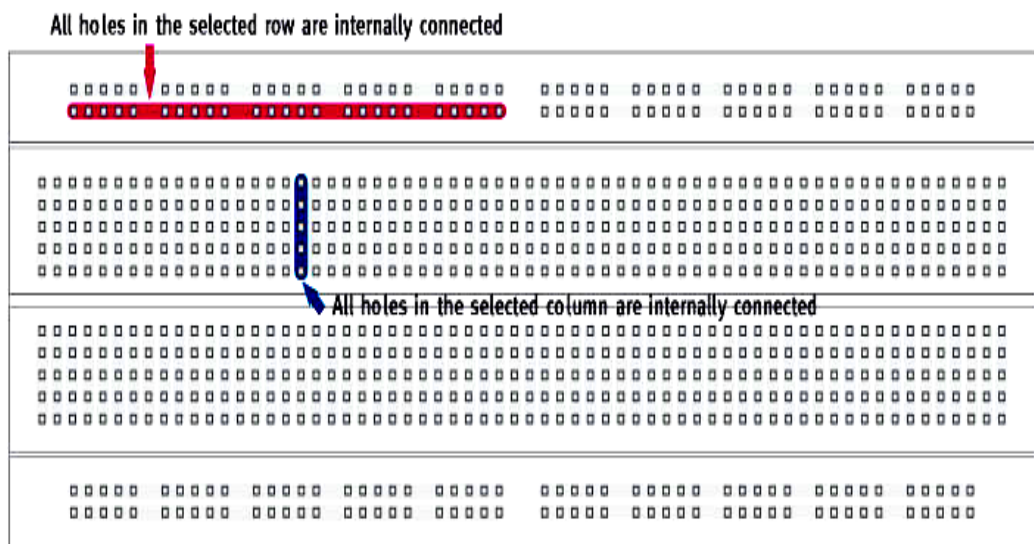


**Fig 3.20: Breadboard**

### 3.8 Thermal Actuation Unit (Cartridge Heater – 230V, 50W):

Cartridge Heater consists of a 50-W stainless-steel cartridge heater used to generate controlled heat for experimental trials. It is driven through the Power Control & Switching Module using appropriate insulation, safety, and temperature monitoring.



Fig 3.21: Cartridge Heater – 230V, 50W

Table 3.16: Electrical Parameters & Physical Construction of Cartridge Heater:

#### Electrical Parameters:

Power	50 WATTS
Voltage	230 V
Current	0.4347
Resistance	1058 ohms
Power Source	AC
Max Temperature	150 °C
Frequency	50 - 60 HZ

#### Physical Construction:

manufacturer model	SRKHP
Heating Element Type	Stainless-steel sheath (cylindrical metal tube)
Size or Diameter	6 MM
Package Dimensions	50 * 6 MM; 103 g
Heating Element internal construction	Nichrome wire wound coil around a ceramic core, Magnesium oxide (MgO) powder fills the space around the coil

### 3.9 Software / Firmware:

- **Arduino IDE** – To program the Arduino board.
- **Libraries:** INA219, Dallas Temperature, SD, Wire, U8g2/U8x8lib, Software Serial (for GSM), Liquid Crystal.

### 3.10 AEM Electrolyzer:

An AEM (Anion Exchange Membrane) electrolyzer splits water using an anion-conducting membrane, generating hydrogen at the cathode and oxygen at the anode while combining the benefits of both PEM and alkaline systems. It operates with non-precious catalysts, supports pure water or low-concentration alkaline feed, and typically runs at moderate temperatures of 40–60°C.



**Fig 3.22: AEM Electrolyzer**

**Table 3.17: AEM Electrolyzer Specifications**

Voltage range	1.7-3v(max)
Current Density	0.5A/cm <sup>2</sup> to 2 A/cm <sup>2</sup>
Cell Fixture	AEM electrolyser
Model	TES-CF-AEM-9-M2
Number of Cells	Single cell
Membrane	Standard -Anion Exchange membrane
Electrolyte	Potassium Hydroxide (KOH) @1M
Flow Configuration	Single side / Dual side
Surface Area	3x3 cm = 9cm <sup>2</sup>
Temperature Range	40°C to 80°C
Cell Torque	6 - 9 Nm (* Based on Loading Conditions)
Cell Weight	1.2 kg (*Loading Conditions)
Cell Dimensions (LXB)	100 mm x 100 mm
Materials of Construction	Stainless steel (SS316)
Sealing Mechanism	Gasket
Leak-Less Cell Design	Yes

# CHAPTER 4

## PROJECT DESIGN & IMPLEMENTATION

### 4.1 Block Diagram of Smart Battery Thermal and Power Management System for PV-Battery-Hydrogen Generation System:

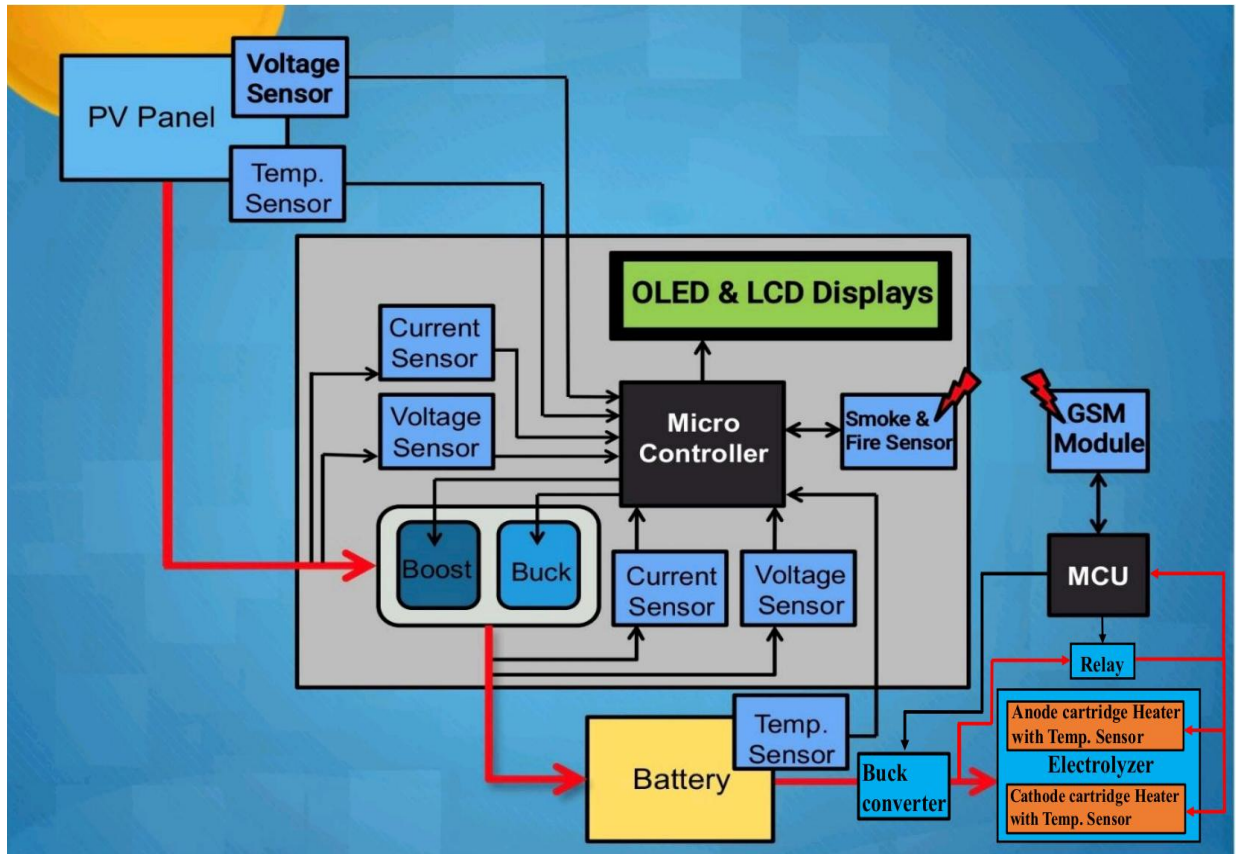


**Fig 4.1: Overall simple Block Diagram of Smart Battery Thermal and Power Management System for PV-Battery-Hydrogen Generation System**

**Smart Battery Thermal and Power Management System** is an integrated solution designed to efficiently manage solar energy, monitor critical parameters, and ensure system safety. It uses a microcontroller to collect real-time data from voltage, current, temperature, and smoke/fire sensors connected to the PV panel, battery, and load. Based on this data, it controls boost and buck converters to regulate power flow for optimal charging and usage. The system displays live readings on LCD/OLED screens and continuously checks for faults like overvoltage, overheating, or fire. If any abnormal condition is detected, the GSM module automatically sends an SMS or makes a call to alert the user, enabling quick response. This project ensures reliable energy management, enhanced safety, and remote fault notification, making it ideal for standalone or remote solar installations.

## 4.2 Equivalent Circuit Model of Smart Battery Thermal and Power Management System:

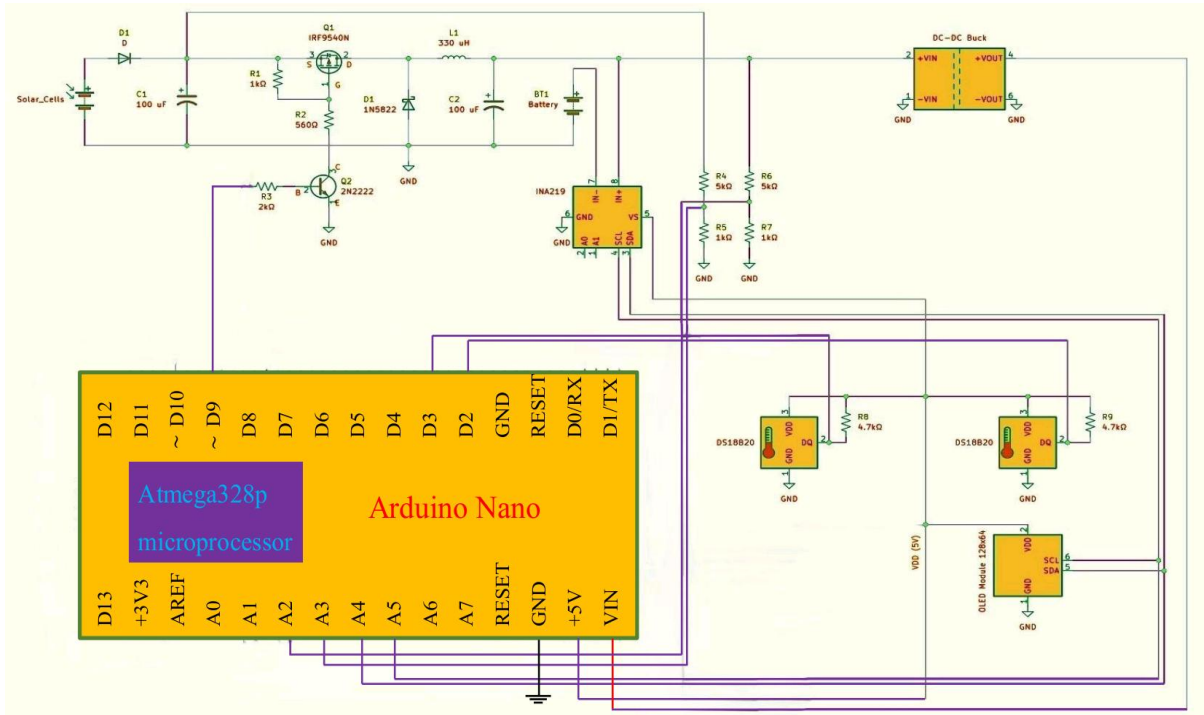


**Fig 4.2: Equivalent Circuit Model of Smart Battery Thermal and Power Management System**

The equivalent circuit model of the Smart Battery Thermal and Power Management System design circuit is shown above this charging system that intelligently manages energy from a photovoltaic (PV) panel to charge a battery safely and efficiently. At the hardware level, the PV panel generates DC electricity, which is first sensed for voltage and current using a voltage divider and the INA219 current sensor module. The sensed parameters are fed to an Arduino Mega, which acts as the system's microcontroller. To condition this raw solar energy, a boost converter circuit comprising a power MOSFET (Q1), inductor (L1), and diode (D1) is controlled via PWM from the Arduino Nano (pin 9). This regulation ensures that adequate voltage is supplied for charging, especially under variable sunlight conditions. The regulated output is directed to charge a 12V battery, with a buck converter added for stepping down voltage for other loads or devices when needed.

The Arduino gathers critical real-time data using additional sensors: two DS18B20 temperature sensors monitor the battery temperature and ambient conditions respectively, while additional voltage sensors track both source (solar) and battery voltages. These inputs feed into a PID-based control algorithm coded inside the Arduino, ensuring dynamic adjustment of the PWM signal that regulates charging current. If conditions become unsafe such as over-voltage (above 12.94V) or overheating (above 40.5°C) the code halts PWM to stop charging and only resumes once safe thresholds are re-entered (e.g., below 12.54V or 38°C). This creates hysteresis logic that prevents rapid switching and enhances safety during borderline conditions.

The software implementation of the control system includes a custom Simple PID class that calculates an optimal PWM duty cycle based on errors between target and actual voltage/current. This allows smoother control of charging current and avoids battery stress or excessive ripple. The system also calculates the state-of-charge (SoC) percentage based on battery voltage and current data, helping modulate the power delivery more gently as the battery nears full charge. In addition to control, the code logs real-time values and acts as a decision-maker to balance performance with battery health, all while working autonomously without requiring user intervention.

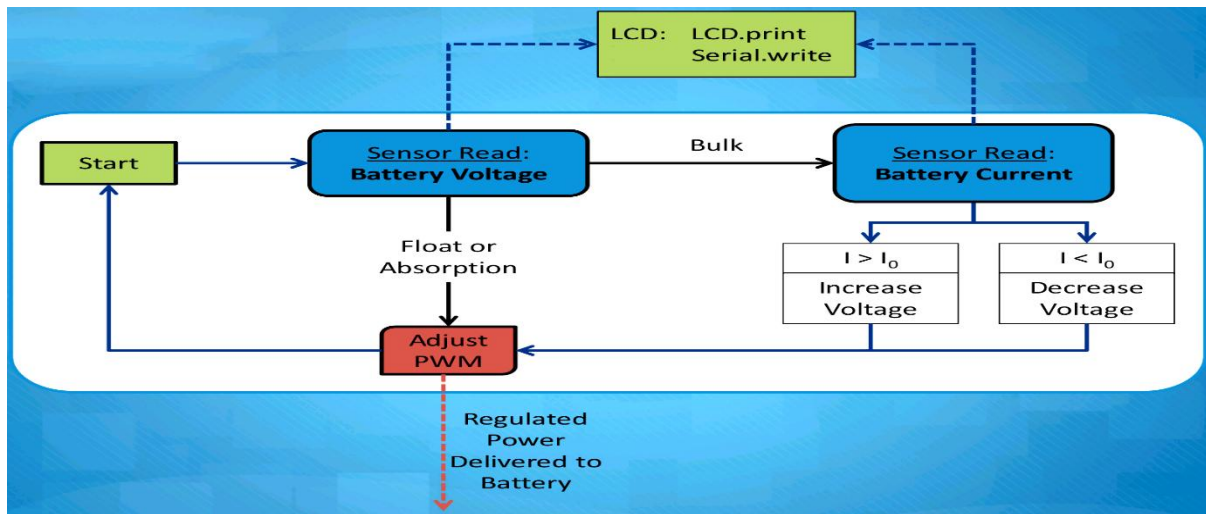


**Fig 4.3: PWM-Based Battery Charging Algorithm with Voltage and Current Feedback**

**Table 4.1: Pin Allocation of Arduino Nano for Components and Sensors**

Component or Sensors	pin	Function
PFET PWM Control	D9	Uses Timer1. PWM (.). Safe because Timer1 is dedicated and not shared with other libraries. This pin controls the PFET (Power MOSFET) gate for battery charging regulation. Keeping it isolated avoids timing conflicts.
Battery Temp Sensor	D2	Measures battery temperature for safety. Initially conflicted with interrupts but works fine now. Connected via One Wire bus (Dallas Temperature /DS18B20 sensor).
Electrolyzer Temp Sensor	D3	Electrolyzer temperature allows independent monitoring and safety-based control (e.g., power shutoff if Electrolyzer temp too high).
I2C OLED Display (U8x8)	A4 & A5	Standard I2C pins: SDA (A4), SCL (A5). Dedicated for OLED display communication. Important: keep reserved for I2C only, don't reassign.
Solar Voltage Input	A3	Analog input pin for sensing voltage (e.g., solar input voltage). Connects to a voltage divider to scale down input to safe Arduino levels (0–5 V).
Battery Voltage Input	A2	Another analog input pin, used for battery voltage measurement. Also goes through a voltage divider for safe measurement.

### 4.3 Equivalent Circuit Model of the Electrolyzer Control Circuit

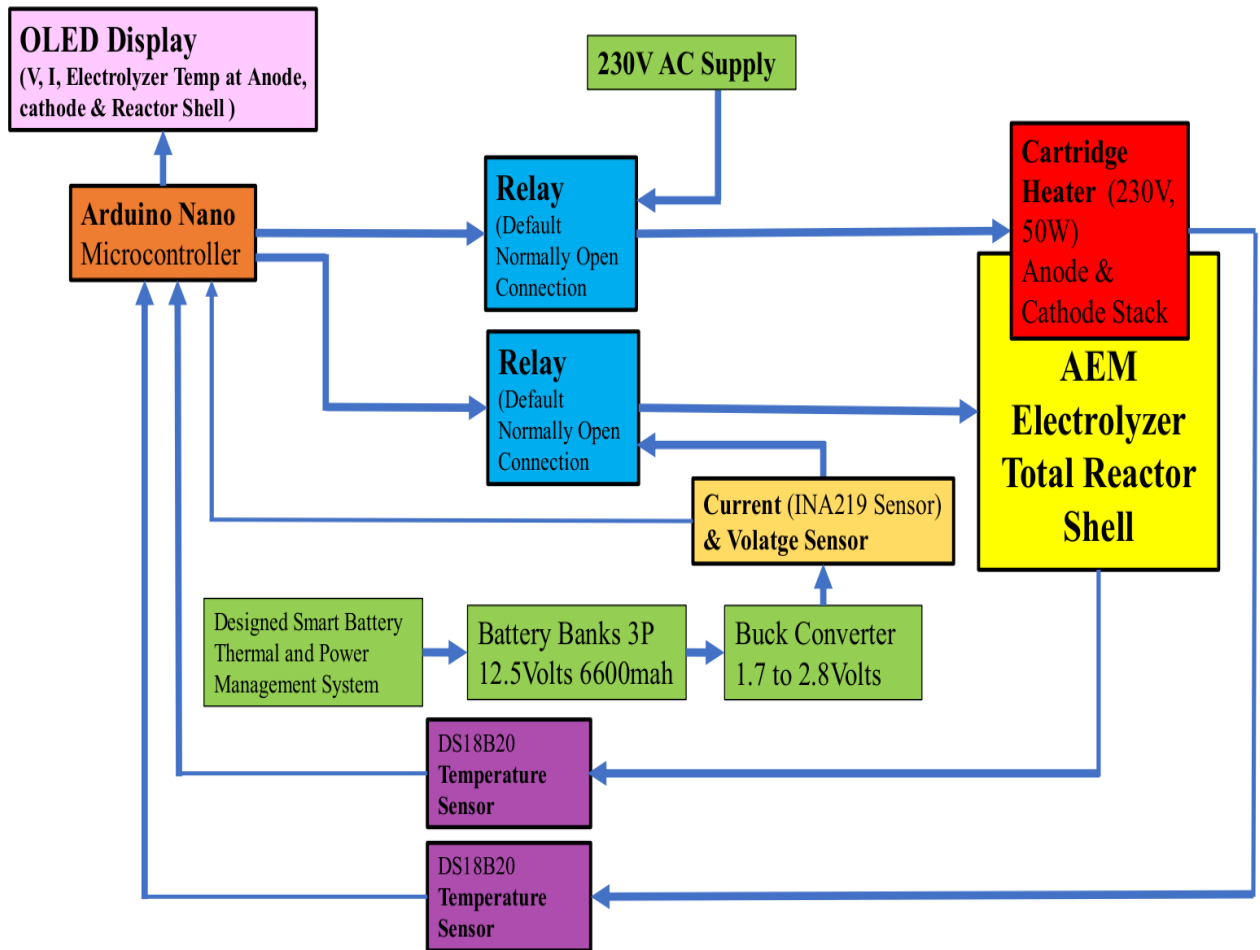


**Fig 4.4: Electrolyzer Control Circuit**

The **Electrolyzer Control Circuit** system developed with the integration of battery-driven DC supply, a controlled AC heating unit (either On or Off), and a complete sensing and monitoring arrangement to operate an AEM electrolyzer under regulated conditions. A 12.5-V, 6600-mAh (3P) battery bank serves as the primary source, protected by a dedicated Smart Battery Thermal and Power Management System that handles cell balancing, temperature supervision, over- and under-voltage protection, and current-limit safeguards before enabling the pack's output. The battery feeds a buck converter, which is adjusted to deliver the required 1.7–2.8 V operating range for the electrolyzer. This output is routed through an INA219 (current sensor) high-side current and voltage monitor, allowing accurate measurement of both the stack voltage and reaction current. All DC connections including those of the buck stage, the INA219 (current sensor), and the Arduino Nano, are kept common to maintain stable referencing. The Arduino, powered by a regulated 5-V rail, manages the sensors, display, and control logic.

The electrolyzer stack receives the regulated low-voltage (1.7-2.8v) DC output, while three DS18B20 digital temperature sensors placed at the anode, cathode, and reactor shell—provide point-wise thermal monitoring over a single one-wire data line with a standard pull-up. An OLED module connected on the I<sup>2</sup>C bus displays real-time temperature, voltage, and current values. To maintain the reactor at its intended operating temperature, a 230-V AC, 50-W cartridge heater is fitted to the reactor body and switched through relays whose default condition is normally open. These relays are controlled by the Arduino and may be substituted with an appropriately rated SSR if smoother AC control or zero-cross switching is required. The mains wiring for the heater routes the live conductor through the relay contacts, while neutral and earth are handled according to electrical-safety practice, supported by suitable fusing and RCD/GFCI protection. The Arduino reads thermal data continuously and applies either hysteresis-based or PID-based decisions to control heater operation, while also enforcing safety cutoffs in the event of abnormal temperature rise or sensor failure.

During startup, the BMS verifies battery integrity before enabling the DC line, after which the Arduino nano (micro controller) initializes the INA219 (Current sensor), detects all DS18B20(temp sensor) devices on the one-wire bus, and confirms by displaying the operation condition of the **Electrolyzer Control Circuit** data in OLED Display. The buck converter is then set to the intended electrolyzer voltage, and the system begins regular monitoring of reaction current, stack voltage, and all three temperature points. The heater is energized only when necessary to achieve the target operating temperature and is immediately shut off if any reading exceeds predefined limits. The arrangement ensures accurate tracking of the electrolyzer's electrical behaviour while maintaining strict thermal control. Additional safety comes from hydrogen venting considerations, proper segregation of mains and low-voltage wiring, common grounding on the DC side, and fuses placed both on the battery and the AC heater line. With these elements combined, the circuit provides a complete, self-contained platform for controlled AEM electrolyzer operation, featuring integrated measurement, thermal regulation, battery protection, and secure switching of the heater load.

#### 4.4 Equivalent Circuit Model of the Circuit Fault Detection and Alert System:

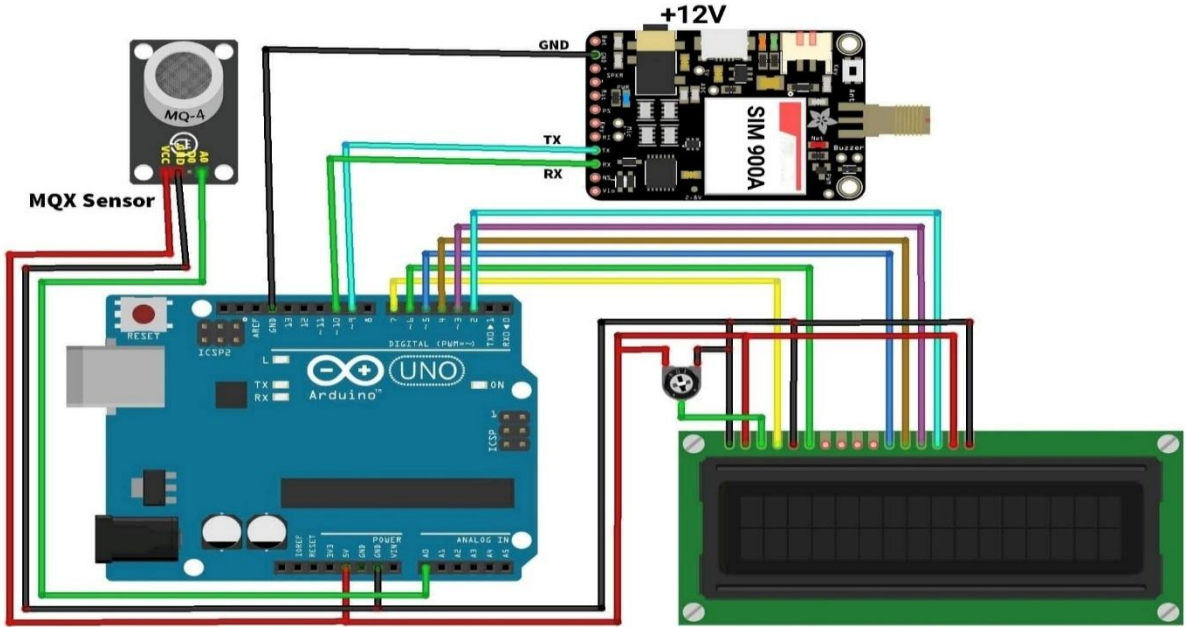


**Fig 4.5: Equivalent Circuit Model of the Circuit Fault Detection and Alert System**

The above equivalent circuit model of the Circuit Fault Detection and Alert System using an Arduino Uno, MQ-4 gas sensor, GSM SIM900A module, and a 16x2 LCD display. The MQ-4 sensor detects combustible gases like methane ( $\text{CH}_4$ ) and outputs an analog signal to the Arduino's A0 pin. The Arduino continuously monitors this signal, and if the gas concentration exceeds a certain threshold (value  $> 500$ ), it considers it a fault condition. The LCD, connected to digital pins 7 through 2, displays real-time status messages such as the current gas level or a warning if a fault is detected. This ensures the user has immediate visual feedback about the circuit or environmental condition. The LCD first shows a welcome message on startup and then updates in real-time during loop execution based on the gas sensor readings.

A standout feature of this system is its remote alert functionality using the SIM900A GSM module, which is connected via software serial (pins 10 for Rx and 11 for Tx). When a fault is detected, the Arduino sends AT commands through the Send Message ( ) function to initialize the module, switch it to text mode, and transmit a predefined SMS alert to a specified phone number. This allows real-time alerts to be sent without relying on internet connectivity. The SIM900A is powered by a separate 12V supply to meet its higher current requirements. The serial monitor also logs live readings and fault messages for debugging or monitoring via a computer. This integration of real-time sensing, display, and GSM communication makes the system highly suitable for applications in industrial safety, electrical labs, and residential gas leak monitoring where both immediate local notification and remote alerts are critical.

## CHAPTER 5

### Results and Discussion

#### 5.1: Developed Smart Battery Thermal and Power Management System for PV-Battery-Hydrogen Generation System:

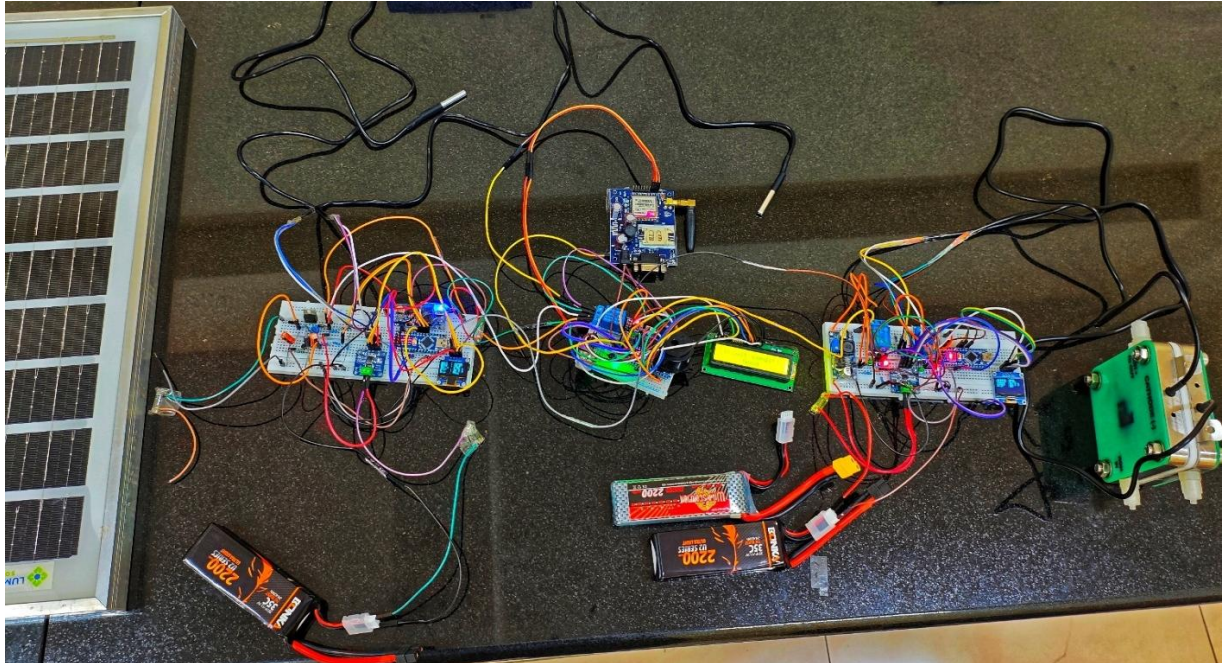


**Fig 5.1: Developed Smart Battery Thermal and Power Management System for PV-Battery-Hydrogen Generation System**

The above fig 5.1 presents a Smart Battery Thermal and Power Management System for a PV-Battery-Hydrogen Generation System capable of handling up to 60 V solar input for a 12 V storage battery while compensating for rapid PV power fluctuations during hydrogen production. The microcontroller-based design integrates precision sensing INA219 for voltage/current measurement and DS18B20 sensors for battery and electrolyzer temperatures combined with closed-loop PID control for both PV charging and AEM electrolyzer heating. The charging PID continuously adjusts current and voltage based on irradiance and battery SOC, with hysteresis protection cutting off charging above 12.94 V or 40.5 °C and restoring it only below 12.54 V or 38 °C. For the electrolyzer, operating ideally between 40–70 °C, a 50 W cartridge heater raises the temperature to 40 °C within minutes, while safety logic disconnects heating above 70 °C and resumes below 65 °C to ensure stable operation. The system incorporates a fire/smoke-based fault detection module that issues LCD alerts, GSM (SIM900A) SMS notifications, and automatic system isolation for immediate hazard response. Together makes automated cold-start capability, precise temperature regulation and strong fault resilience, making the system highly suitable for reliable green hydrogen generation.

## 5.2 Arduino Code for PV Battery Charging with PID Control:

```
#include <TimerOne.h>
#include <Adafruit_INA219.h>
#include <SPI.h>
#include <Wire.h>
#include <OneWire.h>
#include <DallasTemperature.h>
#include <U8x8lib.h>
#include "ChargerClasses.hpp"

#define PFET_PIN 9
#define ONE_WIRE_BUS 2
#define ONE_WIRE_BUS_AMB 3
#define INTERRUPT_PIN 4
#define PWM_INTERRUPT 6

Adafruit_INA219 ina219;
SimplePID voltagePID;
bool charging = true;
bool voltageLockout = false; // For battery over-voltage protection
float t = 0, tn1 = 0, t_record = 0;

U8X8_SSD1306_128X64_NONAME_HW_I2C display(U8X8_PIN_NONE);
OneWire oneWire(ONE_WIRE_BUS), oneWireAmb(ONE_WIRE_BUS_AMB);
DallasTemperature tempSensorB(&oneWire), tempSensorE(&oneWireAmb);
unsigned long lastDisplayUpdate = 0, lastBlinkTime = 0;
const unsigned long displayInterval = 1000;
bool overheatBlink = false;

void setup() {
    pinMode(A2, INPUT); pinMode(A3, INPUT);
    Serial.begin(9600);
    Serial.println("Charger setup started...");
```

```

SPI.begin(); ina219.begin();
Timer1.initialize(100); Timer1.pwm(PFET_PIN, 0);
voltagePID.setParams(0, 0.2e-3, 0, 0, 1);
charging = true;
display.begin();
display.setFont(u8x8_font_chroma48medium8_r);
display.setPowerSave(0);
tempSensorB.begin();
tempSensorE.begin();

// Initial layout (static labels)
display.setCursor(0, 0); display.print("BatI :");
display.setCursor(0, 1); display.print("BatV :");
display.setCursor(0, 2); display.print("Bat% :");
display.setCursor(0, 3); display.print("Sol.V :");
display.setCursor(0, 4); display.print("BatT :");
display.setCursor(0, 5); display.print("E T :");
display.setCursor(0, 6); display.print("Stat :");
}

void loop() {
    float tn = millis() / 1e3, dt = tn - tn1; tn1 = tn; t += dt;
    float iBatt = ina219.getCurrent_mA();

    // ✓ Instant voltage readings
    float vRawA2 = analogRead(A2);
    float vRawA3 = analogRead(A3);
    float vSrc = (vRawA2 * (5.0 / 1023.0)) * 6.0 * 1.04;
    float vBatt = (vRawA3 * (5.0 / 1023.0)) * 6.0 * 1.032;

    // Request and read temperatures
    tempSensorB.requestTemperatures();
    tempSensorE.requestTemperatures();
}

```

```

float tempB = tempSensorB.getTempCByIndex(0);
float tempE = tempSensorE.getTempCByIndex(0);

// 🔋 Battery Over-temperature protection with hysteresis
if (tempB > 40.5) {
    charging = false;
} else if (tempB < 38.0) {
    charging = true;
}

// 🔋 Electrolyzer Over-temperature protection (with hysteresis)
static bool electrolyzerLockout = false; // new state flag
if (tempE > 70.0) {
    electrolyzerLockout = true; // stop power when Electrolyzer exceeds 70 °C
}
else if (tempE < 68.0) {
    electrolyzerLockout = false; // allow power again after cooling
}

// ⚡ Over-voltage protection with hysteresis
if (vBatt > 12.94) {
    voltageLockout = true;
} else if (vBatt < 12.54) {
    voltageLockout = false;
}
float maxCurrent = 500;
int battPercent = constrain((vBatt - 11.54) / (12.54 - 11.54) * 100, 0, 100);
if (battPercent < 50) maxCurrent = 500;
else if (battPercent < 80) maxCurrent = 350;
else if (battPercent < 90) maxCurrent = 200;
else maxCurrent = 100;
float u = voltagePID.evaluate(iBatt, 500, vSrc);
float duty = (charging && !voltageLockout) ? u : 0;

```

```

// Debug info
Serial.print("iBatt: "); Serial.print(iBatt);
Serial.print(" mA, vSrc: "); Serial.print(vSrc);
Serial.print(" V, vBatt: "); Serial.print(vBatt);
Serial.print(" V, tempB: "); Serial.print(tempB);
Serial.print(" C, tempE: "); Serial.print(tempE);
Serial.print(" C, Duty: "); Serial.println(duty * 100);

if (millis() - lastDisplayUpdate >= displayInterval) {
    lastDisplayUpdate = millis();

    int battPercent = constrain((vBatt - 11.54) / (12.54 - 11.54) * 100, 0, 100);
    bool solar = (vSrc > 6.0);

    if (tempB > 40.5 && millis() - lastBlinkTime > 500) {
        overheatBlink = !overheatBlink;
        lastBlinkTime = millis();
    }

    display.setCursor(8, 0); display.print("      "); display.setCursor(8, 0);
    display.print((int)iBatt); display.print("mA");

    display.setCursor(8, 1); display.print("      "); display.setCursor(8, 1);
    display.print(vBatt, 1); display.print("V");

    display.setCursor(8, 2); display.print("      "); display.setCursor(8, 2);
    display.print(battPercent); display.print("%");

    display.setCursor(8, 3); display.print("      "); display.setCursor(8, 3);
    display.print(vSrc, 1); display.print("V");

    display.print(solar ? "\x18" : "X");

    display.setCursor(8, 4);
    if (tempB > 40.5 && overheatBlink) display.print("      ");
    else {
        display.print("      "); display.setCursor(8, 4);
        display.print(tempB, 1); display.print((char)248); display.print("C");
    }
}

```

```

display.setCursor(8, 5); display.print("      "); display.setCursor(8, 5);
display.print(tempE, 1); display.print((char)248); display.print("C");

// ⚠ Display charging status

display.setCursor(8, 6); display.print("      "); display.setCursor(8, 6);
if (!charging) display.print("HOT ");
else if (voltageLockout) display.print("FULL");
else display.print("CHRG");

}

Timer1.pwm(PFET_PIN, duty * 1023); // Apply PWM
}

```

### 5.3 Arduino Code for the Electrolyzer control circuit:

```

#include <Adafruit_INA219.h>
#include <SPI.h>
#include <Wire.h>
#include <OneWire.h>
#include <DallasTemperature.h>
#include <U8x8lib.h>

#define ONE_WIRE_BUS 2
#define ONE_WIRE_BUS_AMB 3

int relayPin7 = 7;      // Relay output to isolate the Anode & Cathode Heating system
int relayPin9 = 9;      // Relay output to isolate the Electrolyzer system
int data = 0;

Adafruit_INA219 ina219;
float t = 0, tn1 = 0, t_record = 0;

U8X8_SSD1306_128X64_NONAME_HW_I2C display(U8X8_PIN_NONE);

OneWire oneWire(ONE_WIRE_BUS), oneWireAmb(ONE_WIRE_BUS_AMB);
DallasTemperature tempSensorA(&oneWire), tempSensorC(&oneWireAmb);

```

```

unsigned long lastDisplayUpdate = 0, lastBlinkTime = 0;
const unsigned long displayInterval = 1000;
bool overheatBlink = false;

void setup() {
    pinMode(A2, INPUT); pinMode(A3, INPUT);
    Serial.begin(9600);
    Serial.println("Electrolyzer setup started...");

    SPI.begin(); ina219.begin();
    pinMode(relayPin7, OUTPUT);
    pinMode(relayPin9, OUTPUT);
    digitalWrite(relayPin7, HIGH); // Relay normally ON (system active)
    digitalWrite(relayPin9, HIGH); // Relay normally ON (system active)

    display.begin();
    display.setFont(u8x8_font_chroma48medium8_r);
    display.setPowerSave(0);

    tempSensorA.begin();
    tempSensorC.begin();

    // Initial layout (static labels)
    display.setCursor(0, 0); display.print("ieletz :");
    display.setCursor(0, 1); display.print("Veletz :");
    display.setCursor(0, 2); display.print("tempA :");
    display.setCursor(0, 3); display.print("tempC :");
    display.setCursor(0, 4); display.print("Stat :");
}

void loop() {
    float tn = millis() / 1e3, dt = tn - tn1; tn1 = tn; t += dt;
    float ieletz = ina219.getCurrent_mA();

```

```

// ✅ Instant voltage readings

float vRawA2 = analogRead(A2);
float vRawA3 = analogRead(A3);
float Velctz = (vRawA2 * (5.0 / 1023.0)) * 6.0 * 1.0;

// Request and read temperatures

tempSensorA.requestTemperatures();
tempSensorC.requestTemperatures();

float tempA = tempSensorA.getTempCByIndex(0);
float tempC = tempSensorC.getTempCByIndex(0);

// --- Electrolyzer 🔌 Overtemperature Protection (Combined Anode & Cathode) ---

if (tempC > 50.5 || tempA > 50.5) {
    digitalWrite(relayPin7, HIGH); // Isolate Electrolyzer
} else if (tempC < 48.0 && tempA < 48.0) {
    digitalWrite(relayPin7, LOW); // Allow power again
}

// 🔌 + 🚧 Combined Electrolyzer Temperature & Over-voltage Protection

if (tempA > 60.5 || tempC > 60.5 || Velctz > 2.2) {
    digitalWrite(relayPin9, HIGH); // Isolate the Electrolyzer system
} else if (tempA < 48.0 && tempC < 48.0 && Velctz < 1.54) {
    digitalWrite(relayPin9, LOW); // Allow Electrolyzer operation
}

float maxCurrent = 2000;

// Debug info

Serial.print("ielctz: "); Serial.print(ielctz);
Serial.print(" mA, Velctz: "); Serial.print(Velctz);
Serial.print(" V, tempA: "); Serial.print(tempA);
Serial.print(" C, tempC: "); Serial.print(tempC);

if (millis() - lastDisplayUpdate >= displayInterval) {
    lastDisplayUpdate = millis();
}

```

```

if (tempA > 50.5 && millis() - lastBlinkTime > 500) {
    overheatBlink = !overheatBlink;
    lastBlinkTime = millis();
}

else if (tempC > 50.5 && millis() - lastBlinkTime > 500)
{ overheatBlink = !overheatBlink;
lastBlinkTime = millis(); }

display.setCursor(8, 0); display.print("      "); display.setCursor(8, 0);
display.print((int)ieletz); display.print("mA");

display.setCursor(8, 1); display.print("      "); display.setCursor(8, 1);
display.print(Velctz, 1); display.print("V");

display.setCursor(8, 2);
if (tempA > 50.5 && overheatBlink) display.print("      ");
else {
    display.print("      "); display.setCursor(8, 2);
    display.print(tempA, 1); display.print((char)248); display.print("C");
}
}

display.setCursor(8, 3);
if (tempC > 50.5 && overheatBlink) display.print("      ");
else {
    display.print("      "); display.setCursor(8, 3);
    display.print(tempC, 1); display.print((char)248); display.print("C");
}

// ⚠ Display Electrolyzer status

display.setCursor(8, 4); display.print("      "); display.setCursor(8, 4);
display.print("ON");
}

}

```

## **5.4 Arduino Code for the Circuit Fault Detection and Alert System:**

```
#include <LiquidCrystal.h>
LiquidCrystal lcd(7, 6, 5, 4, 3, 2);
#include <SoftwareSerial.h>
SoftwareSerial mySerial(10, 11); // GSM module
int gasValue = A0;      // Gas/smoke sensor analog input
int flameSensor = 8;    // Flame sensor digital input
int relayPin = 9;       // Relay output to isolate the system
int data = 0;
void setup()
{ randomSeed(analogRead(0));
  mySerial.begin(9600); // GSM Module baud rate
  Serial.begin(9600); // Serial monitor
  lcd.begin(16, 2);
  pinMode(gasValue, INPUT);
  pinMode(flameSensor, INPUT);
  pinMode(relayPin, OUTPUT);
  digitalWrite(relayPin, HIGH); // Relay normally ON (system active)
  lcd.print(" Crkt fault detection system ");
  delay(3000);
  lcd.clear();
}
void loop()
{ data = analogRead(gasValue);
  int flameState = digitalRead(flameSensor); // LOW = fire detected
  Serial.print("Crkt condition: ");
  Serial.println(data);
  // Case 1: Flame detected
  if (flameState == LOW) {
    digitalWrite(relayPin, LOW); // Isolate the system
    SendMessage("Circuit Fault Detected! Check the circuit & solar panel is Isolated.");
    Serial.println("Circuit Fault Detected!");
    lcd.clear();
  }
}
```

```

lcd.setCursor(0, 0);
lcd.print("Crkt Fault Detected ");
lcd.setCursor(0, 1);
lcd.print("solar panel isolated");
delay(2000);
lcd.clear();
lcd.setCursor(1, 0 );
lcd.print("SMS Sent");
lcd.setCursor(1, 1 );
lcd.print("Check the Ckrt");
delay(20000);
}

// Case 2: fault detected
else if (data > 500) {
    digitalWrite(relayPin, LOW); // Isolate the system
    SendMessage("Circuit Fault Detected! Check the circuit & solar panel is Isolated.");
    Serial.println("Circuit Fault Detected!");
    lcd.clear();
    lcd.setCursor(0, 0);
    lcd.print("Crkt Fault Detected ");
    lcd.setCursor(0, 1);
    lcd.print("solar panel isolated");
    delay(2000);
    lcd.clear();
    lcd.setCursor(1, 0 );
    lcd.print("SMS Sent");
    lcd.setCursor(1, 1 );
    lcd.print("Check the Ckrt");
    delay(3000);
}

// Case 3: Normal condition
else {
    digitalWrite(relayPin, HIGH); // Keep system active
    Serial.println("Circuit condition Good");
}

```

```

lcd.clear();
lcd.setCursor(0, 0);
lcd.print("Circuit condition");
lcd.setCursor(0, 1);
lcd.print("    Good    ");
delay(3000); }

lcd.clear();}

void SendMessage(String text) {
Serial.println("Sending SMS...");
mySerial.println("AT+CMGF=1");
delay(1000);
mySerial.println("AT+CMGS=\"+918351988928\"\r");
delay(1000);
mySerial.println(text);
delay(100);
mySerial.println((char)26); //
delay(2000);
}

```

## **5.5 All Experimental Data of Developed Smart Battery Thermal and Power Management System for PV-Battery-Hydrogen Generation System:**

To evaluate the Electrolyzer behaviour, battery behaviour, thermal response, power-regulation accuracy, and protection performance of the developed Smart Battery Thermal and Power Management System for the PV-Battery-Hydrogen Generation System, a five-hour controlled test was conducted in which every critical parameter including battery voltage, charging and load current, multi-point temperature readings, buck-converter output, and the system's reaction to rapid PV-power fluctuations was continuously recorded. The collected figures and tables summarize these results, capturing trends in voltage progression, stability of the control algorithm, and the behaviour of the thermal-management features under varying load and ambient conditions. All transient events such as current spikes, voltage dips, and temperature deviations were also logged, providing complete experimental evidence of the system's operational stability, charging accuracy, and integrated protection capability during operation within the hydrogen-generation framework:

**Table 5.1: Experimental Data of Solar Panel (60w) and SBT&PMS Input-Output Characteristics with Respect to Duty Cycles with a Fixed Solar Irradiation (Halogen Lamp)**

S.No.	Fixed Solar Irradiation		Solar Panel		SBT&PMS		Duty Cycle
	Btu/hr/square foot	Watt/square meter	Input Voltage(V)	Input Current(A)	Output Voltage(V)	Output Current(A)	
1.	120	378.550	1	0	0	0	0
2.	120	378.550	2	0.5	0	0	0
3.	120	378.550	4	0.7	0	0	0
4.	120	378.550	5	0.9	0	0	0
5.	120	378.550	6	0.8	0	0	0
6.	120	378.550	9	0.96	8.5	0.72	0.94
7.	120	378.550	10	1.10	9.2	0.86	0.92
8.	120	378.550	11	1.12	10.46	0.93	0.95
9.	120	378.550	12	1.13	11.52	0.98	0.96
10.	120	378.550	13	1.15	12.51	1.10	0.96
11.	120	378.550	14	1.19	12.6	1.12	1.11
12.	120	378.550	15	1.21	12.7	1.28	0.84
13.	120	378.550	16	1.23	12.8	1.41	0.80
14.	120	378.550	17	1.25	12.82	1.39	0.75
15.	120	378.550	18	1.27	12.83	1.43	0.71
16.	120	378.550	19	1.28	12.84	1.52	0.67
17.	120	378.550	20	1.32	12.85	1.59	0.64
18.	120	378.550	21	1.31	13.16	1.62	0.61
19.	120	378.550	22	1.30	13.37	1.68	0.585
20.	120	378.550	23	1.33	13.88	1.73	0.56
21.	120	378.550	24	1.38	13.89	1.81	0.537
22.	120	378.550	25	1.37	13.90	1.92	0.516
23.	120	378.550	26	1.35	13.95	1.96	0.498
24.	120	378.550	27	1.28	14.21	1.98	0.489
25	120	378.550	28	1.24	14.28	1.95	0.474
25	120	378.550	29	1.18	14.32	1.98	0.459
27	120	378.550	30	1.12	14.44	1.96	0.451
28	120	378.550	31	1.09	14.40	1.97	0.448
29	120	378.550	32	1.19	14.42	1.94	0.431

Three-stage battery charging process used in Smart Battery Thermal and Power Management System for Photovoltaic Battery Charging:

1. Bulk Stage
2. Absorption Stage
3. Float Stage

**Table 5.2: Voltage Profile of Solar Panel and 12v 6600mah Battery (3p Connection) with respective to Time 5hrs**

Time(hrs)	Solar Panel Voltage(V)	Battery Voltage(V)
0	18.9	9.11
0.25	17.64	9.5
0.5	17.8	10.12
0.75	17.4	10.4
1	17.1	10.55
1.25	16.9	10.93
1.5	16.6	11.15
1.75	16.45	11.29
2	16.31	11.42
2.25	16.28	11.53
2.5	16.19	11.91
2.75	16.23	11.95
3	16.35	12.04
3.25	16.39	12.22
3.5	16.42	12.38
3.75	16.49	12.41
4	16.56	12.44
4.25	16.71	12.52
4.5	16.9	12.61
4.75	17.15	12.69
5	17.3	12.78

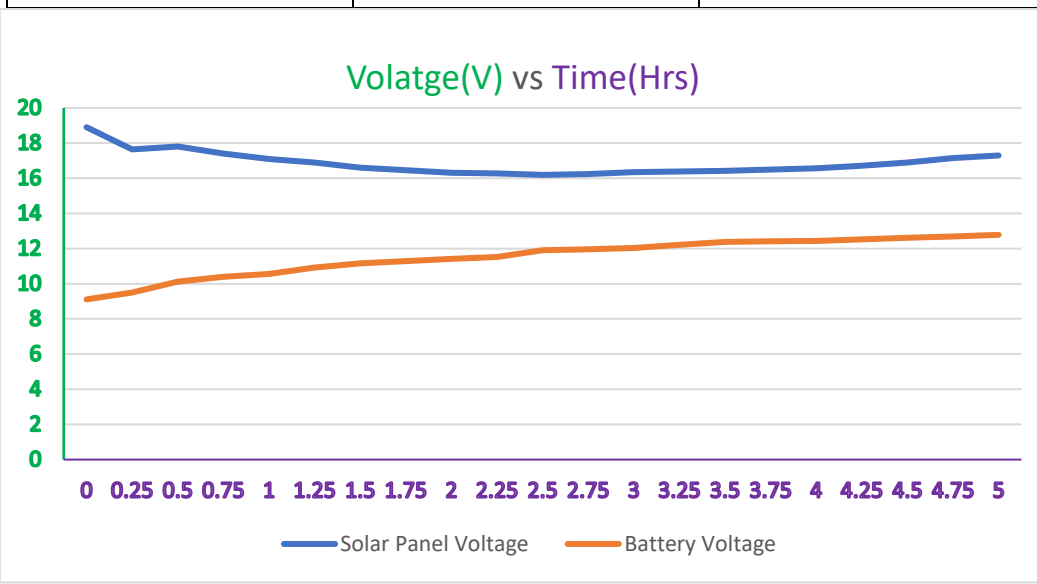


**Fig 5.2: Voltage Profile of Solar Panel and Battery vs Time**

**Table 5.3: Current Profile of 12v 6600mah Battery with respective to Time**

Time(hrs)	Instant Current during Battery charging (Amps)
0	1.95
0.25	1.896
0.5	1.96
0.75	1.9
1	1.959
1.25	1.96
1.5	1.955
1.75	1.911
2	1.953
2.25	1.95
2.5	1.86
2.75	1.755
3	1.64
3.25	1.43
3.5	1.34
3.75	0.643
4	0.547
4.25	0.289
4.5	0.254
4.75	0.133
5	0.102

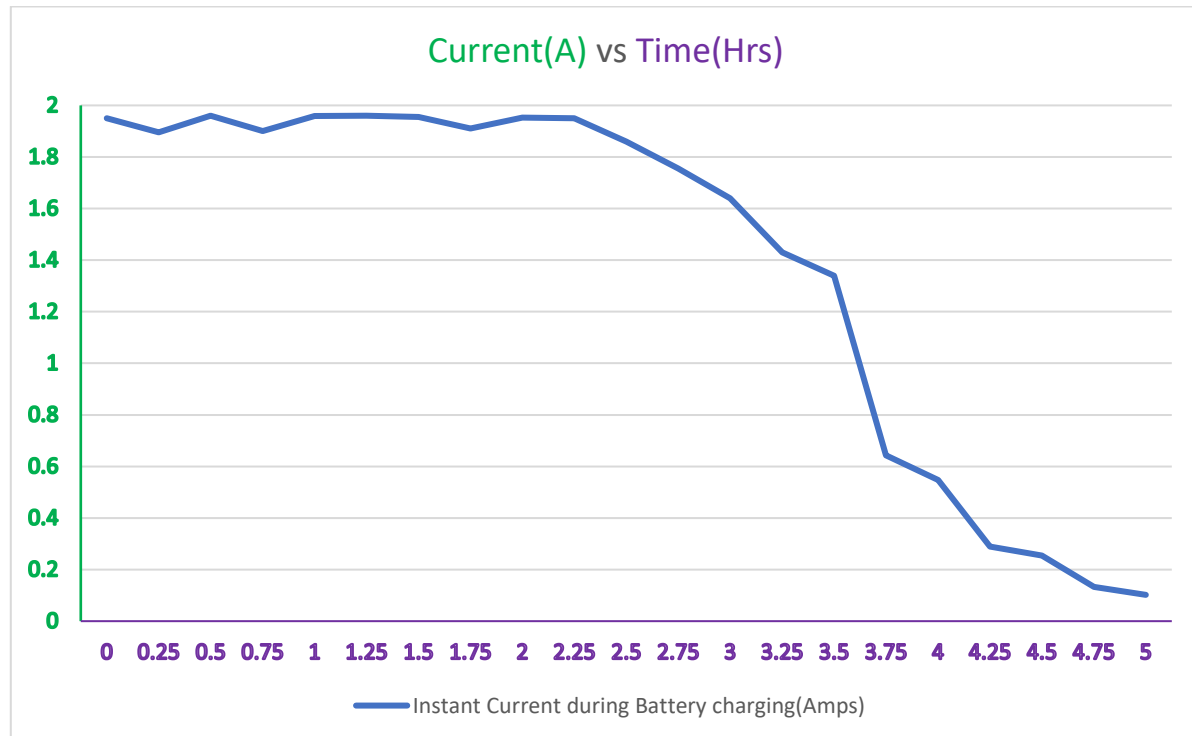


**Fig 5.3: Current Profile of Battery vs Time**

**Table 5.4: SOC (%) Profile of 12v 3\*2200mah Battery (3cells in parallel) with respective to Time**

$$SOC = \frac{\text{Capacity Remaining}}{\text{Total Capacity}} * 100 * \text{hrs}$$

time_h	12v 3*2200mah Battery SOC(%)
0	0
0.25	5.714
0.5	14.429
0.75	19.143
1	25.857
1.25	29.571
1.5	37.286
1.75	40
2	48.714
2.25	51.429
2.5	57.143
2.75	62.857
3	70.571
3.25	74.286
3.5	85.9
3.75	86.869
4	89.642
4.25	91.537
4.5	95.293
4.75	97.358
5	99.04

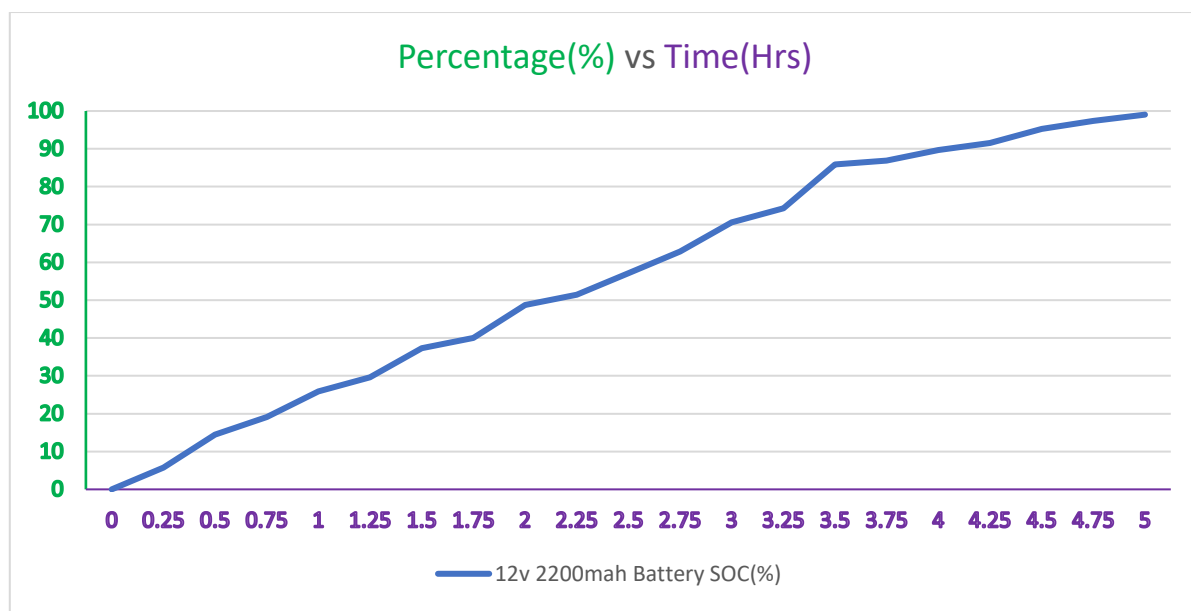


**Fig 5.4: SOC (%) Profile of 12v 2200mah Battery vs Time**

## Over Temperature Protection for Battery:

**Table 5.5: Voltage Response to Battery Over temperature Condition**

Battery Temperature	Solar Panel Voltage	Battery Voltage
32.5	18	13.8
32.5	17.1	13.78
32.5	16.4	13.78
32.5	16.2	13.79
38.9	16.1	13.81
41	16	13.79
42	0	12.58
42.5	0	12.58
39	0	12.58
38	15.4	12.92
35	15.5	13.2
33	16	13.4
32.5	16.9	13.5

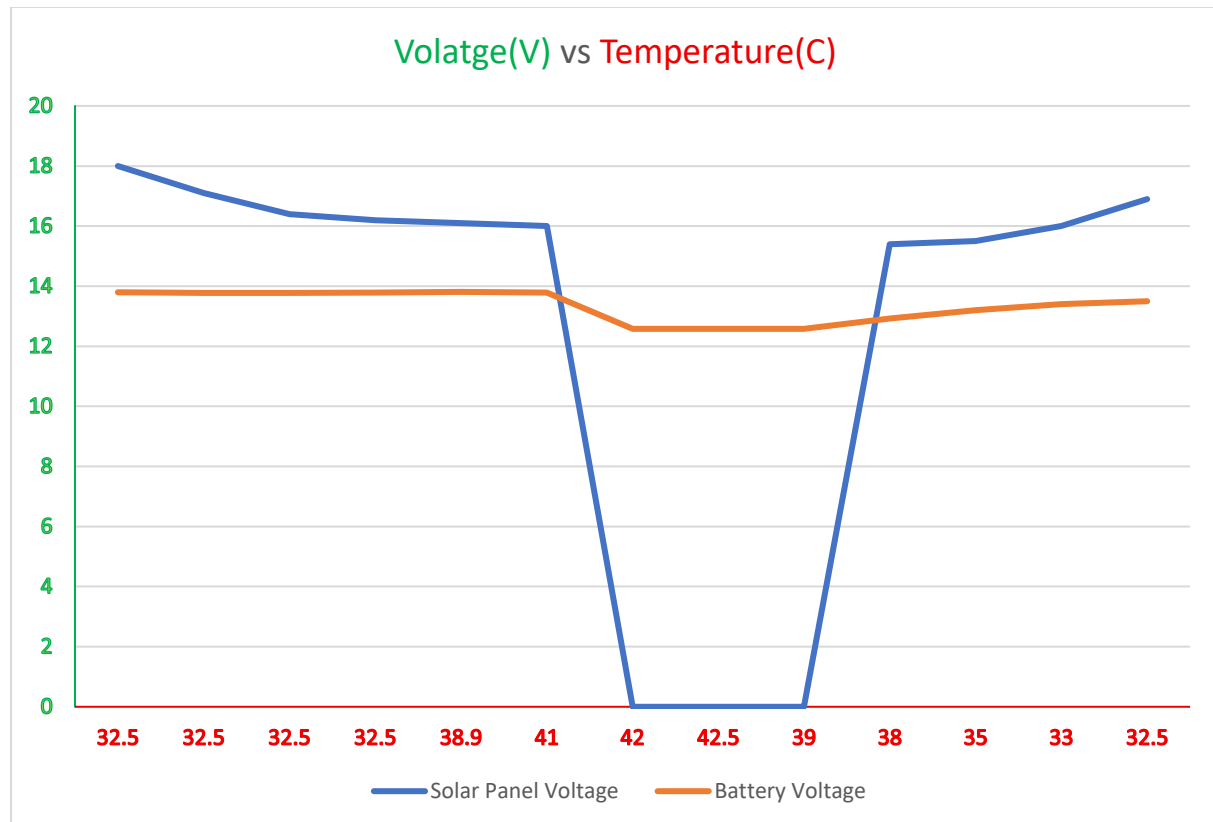


**Fig 5.5: Voltage Response to Battery Overtemperature Condition**

**Table 5.6: Over Temperature Protection for AEM Electrolyzer:**

Electrolyzer Temperature	Applied Voltage to Cartridge Heater(AC 230v)	Electrolyzer Voltage
67.5	232	2.1
68	232	2.2
67.8	232	2.2
68.5	232	2.1
69	232	2.2
70	0	2
70	0	0
70.9	0	0
69.8	0	0
68.3	0	0
66.9	232	0.1
64.6	232	2
66	232	2.2
65.8	232	2.3
66.1	232	2.4

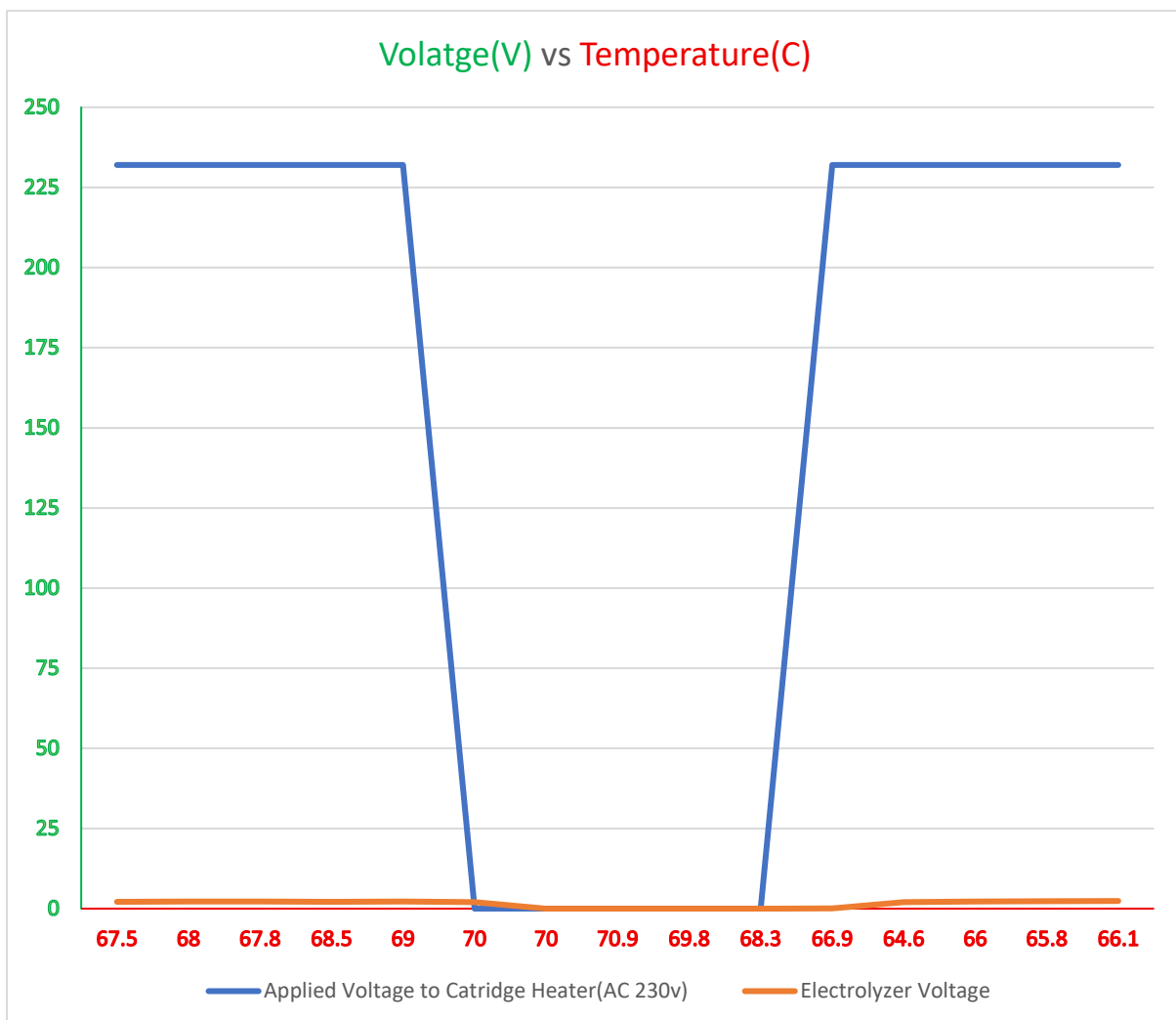


**Fig 5.6: Voltage Response to AEM Electrolyzer Overtemperature Condition**

## 5.6 AEM Electrolyzer Running Characteristics (V, I and P) for 5 min:

AEM Electrolyzer was operated for five hours under controlled conditions. Throughout the test when we Applied max voltage of V) achieved voltage & current at electrolyzer at multiple points has recorded, buck-converter output, and responses to power fluctuations were recorded.

**Table 5.7: AEM Electrolyzer Running Characteristics (V, I and P) for 5min or 300sec**

Time(5min)	voltage(v)	current (A)	Power(W)
0	2.65	2.65	5.25
12.5	2.57	2.26	5.25
25	2.55	2.19	5.25
37.5	2.53	2.15	5.25
49	2.53	2.15	5.25
50	2.6	2.8	7
62.5	2.595	2.71	7
75	2.585	2.6	7
87.5	2.585	2.6	7
99	2.585	2.6	7
100	2.7	3.2	9
112.5	2.69	3.11	9
125	2.685	3	9
137.5	2.685	3	9
149	2.685	3	9
150	2.8	3.8	11.5
162.5	2.795	3.75	11.5
175	2.785	3.7	11.5
187.5	2.785	3.7	11.5
199	2.785	3.7	11.5
200	2.9	4.6	13.75
212.5	2.895	4.55	13.75
225	2.885	4.5	13.75
237.5	2.885	4.5	13.75
249	2.885	4.5	13.75
250	3	5	15
262.5	2.995	4.95	15
275	2.985	4.9	15
287.5	2.985	4.9	15
300	2.985	4.9	15

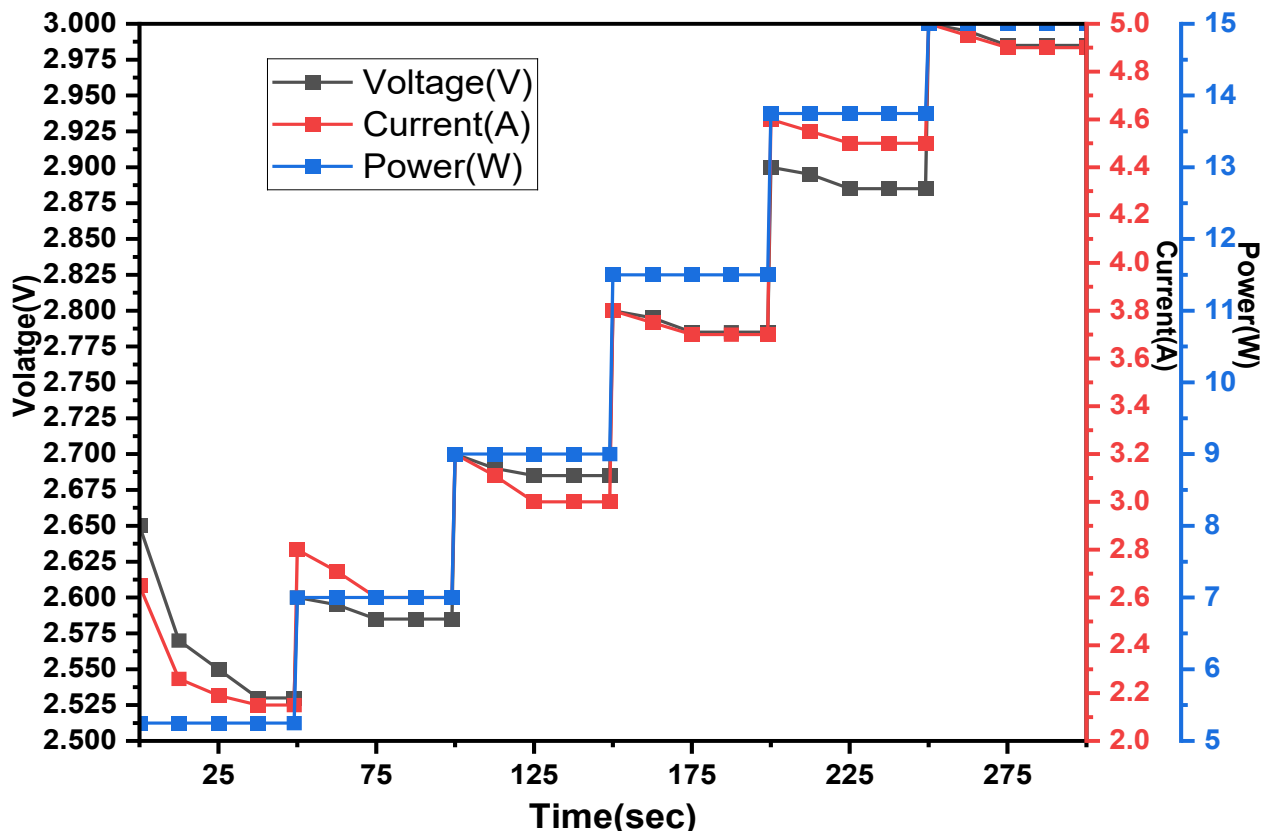


**Fig 5.7: AEM Electrolyzer Running Characteristics for Volatage(V), Current(A), Power(W) with respective to Time(Sec)**

Applied Voltage(V)	Achieved Voltage(V)
3V	2.985V
Applied Current(A)	Achieved Current(A)
5A	4.9A

#### **Observation from Graph & table after Running the AEM Electrolyzer:**

The plotted data illustrates how the AEM electrolyzer responds when voltage, current, and power are increased in a stepped manner over a 300-second run. Instead of using a linear rise, the experiment is carried out through 18 timed intervals where each parameter is held steady for a short period and then raised to the next level. As seen in the graph, voltage progresses from roughly 2.50 V to about 2.95 V, current moves from 2 A up to 5 A, and power correspondingly increases from around 5 W to nearly 15 W. Each flat segment represents a stable set point at which the electrolyzer is allowed to settle, while the sharp vertical transitions show the moments when the next step is applied. This pattern closely matches the actual behaviour observed during the running test, where the system is intentionally kept at fixed operating levels before shifting upward, helping to clearly identify how the electrolyzer stabilizes, how quickly it responds after each increment, and how the achieved values (2.985 V and 4.9 A) compare with the applied 3 V and 5 A set points.

## **5.7 Theoretical Calculation on Hydrogen Generated by AEM Electrolyzer**

### **Running Characteristics:**

**We know that**

Moles of Hydrogen per second(mol/s):

$$N_{H_2} = \frac{nI}{2F}$$

Hydrogen in Litres per minute(L/min):

$$V_{H_2} = N_{H_2}(\text{mol/s}) * 60$$

No. of electrolyzers, n = 1

Faradays Constant, F = 96485 C/mol

#### **(i) At 50Sec:**

Voltage = 2.53V

Current = 2.15A

Moles of Hydrogen per second:

$$N_{H_2} = \frac{1*2.15}{2*96485} = 0.0000111416 \text{ mol/s}$$

Hydrogen in Litres per minute:

$$V_{H_2} = 0.0000111416 \text{ mol/s} * 60 = 0.0006685 \text{ L/min}$$

#### **(ii) At 100Sec:**

Voltage = 2.585V

Current = 2.6A

Moles of Hydrogen per second:

$$N_{H_2} = \frac{1*2.6}{2*96485} = 0.00001347 \text{ mol/s}$$

Hydrogen in Litres per minute:

$$V_{H_2} = 0.00001347 \text{ mol/s} * 60 = 0.0008084 \text{ L/min}$$

#### **(iii) At 150Sec:**

Voltage = 2.685V

Current = 3A

Moles of Hydrogen per second:

$$N_{H_2} = \frac{1*2.685}{2*96485} = 0.00001391 \text{ mol/s}$$

Hydrogen in Litres per minute:  $V_{H_2} = 0.00001391 \text{ mol/s} * 60 = 0.0008348 \text{ L/min}$

**(iv) At 200Sec:**

Voltage = 2.785V

Current = 3.7A

Moles of Hydrogen per second:

$$N_{H_2} = \frac{1*3.7}{2*96485} = 0.00001937 \text{ mol/s}$$

Hydrogen in Litres per minute:

$$V_{H_2} = 0.00001937 \text{ mol/s} * 60 = 0.0011624 \text{ L/min}$$

**(v) At 250Sec:**

Voltage = 2.885V

Current = 4.5A

Moles of Hydrogen per second:

$$N_{H_2} = \frac{1*4.5}{2*96485} = 0.00002331 \text{ mol/s}$$

Hydrogen in Litres per minute:

$$V_{H_2} = 0.00002331 \text{ mol/s} * 60 = 0.001399 \text{ L/min}$$

**(vi) At 300Sec:**

Voltage = 2.985V

Current = 4.9A

Moles of Hydrogen per second:

$$N_{H_2} = \frac{1*4.9}{2*96485} = 0.00002539 \text{ mol/s}$$

Hydrogen in Litres per minute:

$$V_{H_2} = 0.00002539 \text{ mol/s} * 60 = 0.00152 \text{ L/min}$$

**Observation Based on the theoretical hydrogen-generation calculations** and the recorded AEM electrolyzer running characteristics, we can conclude that the applied voltage–current steps produce reaction currents consistent with Faraday’s law, confirming that the electrolyzer generates hydrogen at the theoretically expected rate for each operating level. The smooth current stabilization, proportional rise in power, and absence of unstable spikes demonstrate efficient electrochemical behaviour, meaning the system converts electrical input into hydrogen output with predictable performance.

### 5.8 Circuit Fault Detection and Alert System through SMS:

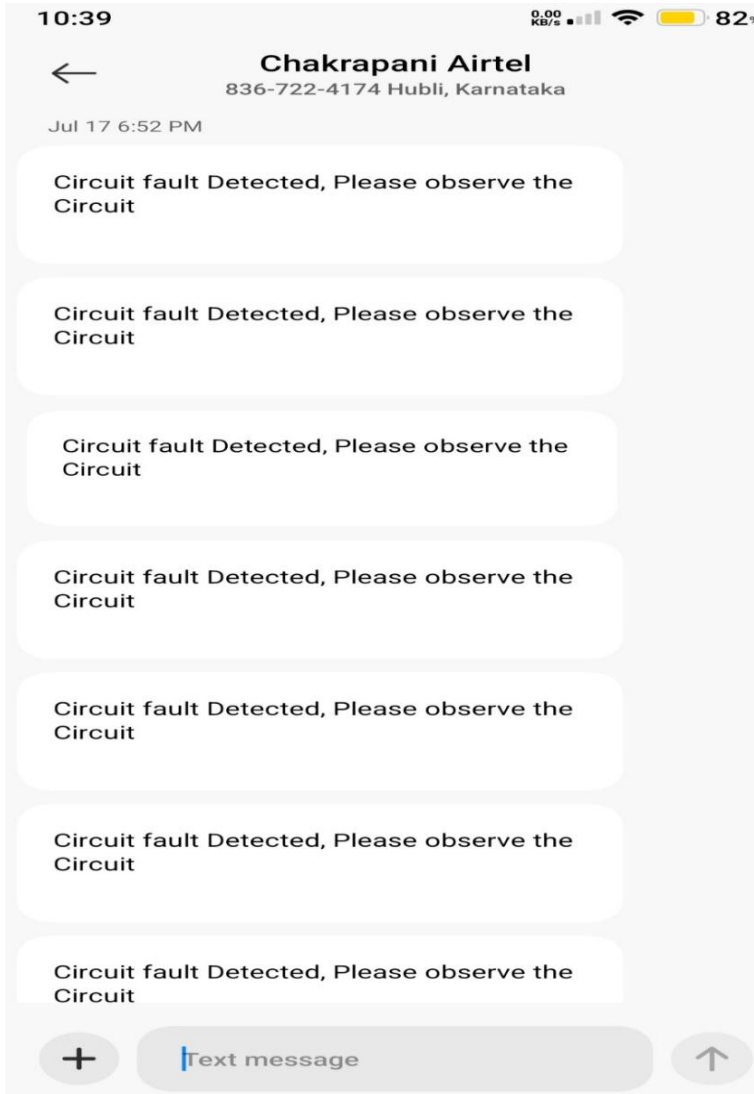


**Fig 5.8: SMS-Based Alert Notification for Circuit Fault Detection**

The SMS-Based Alert Notification for Circuit Fault Detection provides real-time supervision of the PV-Battery-Hydrogen Generation System and ensures rapid operator response during faults. During testing, the system successfully detected over-current conditions above 2.5 A flowing into battery during charging period, voltage deviations beyond  $\pm 5\%$ , and thermal rises above 45 °C, with SMS alerts delivered to humans to take direct action on the particular location. Safety mechanisms include hardware over-temperature cut-off when the electrolyzer exceeds 70 °C, resuming only after temperatures fall below 65 °C, preventing operation until stable conditions are restored. The integrated fire/smoke sensor triggers LCD warnings, GSM (SIM900A) SMS notifications, and automatic system isolation during abnormal events, ensuring fast human intervention and enhancing overall operational safety and reliability.

# CHAPTER 6

## 6.1 SUMMARY AND CONCLUSION

The Smart Battery Thermal and Power Management System integrate solar charging and fault detection systems highlights the potential of embedded technology in addressing critical energy management and safety challenges. The smart solar charger, with its combination of hardware sensors, real-time monitoring via OLED, and PID-based control, ensures efficient, safe, and autonomous battery charging even under fluctuating solar conditions. It incorporates protective features like temperature and voltage hysteresis, making it robust for renewable energy applications. Meanwhile, the Circuit Fault Detection and Alert System offer a practical safety solution, detecting hazardous gas leaks or circuit anomalies and immediately alerting users through both visual LCD feedback and GSM-based SMS notifications. Together, these projects showcase how microcontroller-based systems can improve both operational efficiency and safety in diverse scenarios.

In the future, these systems can be enhanced with additional Real-time DS18B20 data monitors ambient, and electrolyzer temperatures, while voltage feedback ensures precise regulation. For the AEM electrolyzer (40 - 70 °C), a 50 W cartridge heater raises temperature to 40 °C within 5 - 10 min under insulation, with a microcontroller-driven solid-state relay in time-proportioning mode maintaining ±0.5 - 1 °C stability. And to design integrated with automated cold-start capability, precise thermal control and regulation, efficient PV power utilization, and robust fault protection, thereby enhancing the operational efficiency of green hydrogen production and contributing to sustainable energy storage solutions for off-grid and renewable applications that prioritize efficiency, safety, and resilience.

## 6.2 FUTURE SCOPE

The present system offers a strong foundation for PV-powered hydrogen generation; however, several advancements can significantly enhance efficiency, durability, and overall operational performance. A key direction for future development is the replacement of high-cost platinum–iridium catalysts with low-cost carbon (ultra-thin, highly porous)–coated nickel foam electrodes in the AEM electrolyzer. This modification is expected to improve electrical conductivity, increase active surface area, strengthen electrode stability, and support better retention of catalytic material during prolonged electrolysis. Integrating such advanced porous electrodes can reduce system cost while simultaneously enhancing hydrogen production efficiency and long-term operational reliability.

In parallel, the Smart Battery Thermal and Power Management System can be further optimized to better coordinate with PV-battery-hydrogen operation. Future improvements may include refining the control algorithms to achieve faster response during sudden PV fluctuations, enabling more accurate power flow balancing between the PV array, battery pack, and electrolyzer. Enhancing the thermal monitoring architecture—with adaptive cooling strategies and predictive temperature control—will strengthen battery safety, reduce degradation, and support stable charging in dynamic outdoor conditions. Additional improvements like real-time SoC/SoH estimation, cloud-based data logging, and fault-tolerant power routing can make the system more intelligent and autonomous.

Overall, integrating advanced electrode materials with an optimized thermal-power management will move the system closer to a automated PV-Battery-Hydrogen Generation ecosystem capable of high efficiency, lower cost, and reliable long-duration renewable hydrogen production.

## CHAPTER 7

### Reference

- [1] Awad M, Mahmoud MM, Elbarbary ZMS, Mohamed Ali L, Fahmy SN, Omar AI (2023) Design and analysis of photovoltaic/wind operations at MPPT for hydrogen production using a PEM electrolyzer: Towards innovations in green technology. Published on July 20, 2023. At PLoS ONE 18(7): e0287772. <https://doi.org/10.1371/journal.pone.0287772>
- [2] Mustafa Ergin Sahin. A photovoltaic powered electrolysis converter system with maximum power point tracking control. Published on 13 February 2020. At International Journal of Hydrogen Energy. <https://doi.org/10.1016/j.ijhydene.2020.01.162>
- [3] Kikuchi Y, Ichikawa T, Sugiyama M, Koyama M. Battery-assisted low-cost hydrogen production from solar energy: rational target setting for future technology systems. Published on 13 December 2018. At international journal of hydrogen energy 44 (2019) 1451 e1465. <https://doi.org/10.1016/j.ijhydene.2018.11.119>
- [4] Cai X, Lin R, Xu J, Lu Y. Construction and analysis of photovoltaic directly coupled conditions in PEM electrolyzer. Published on 24 December 2021. At Int J Hydrogen Energy Feb. 2022;47(10): 6494–507. <https://doi.org/10.1016/j.ijhydene.2021.12.017>
- [5] Raj Kapur Kumar, Paulson Samuel. Designing a hydrogen generation system through PEM water electrolysis with the capability to adjust fast fluctuations in photovoltaic power. Published on 29 July 2024. At International Journal of Hydrogen Energy 82 (2024) 1–10. <https://doi.org/10.1016/j.ijhydene.2024.07.376>
- [6] Yodwong B, Guilbert D, Phattanasak M, Kaewmanee W, Hinaje M, Vitale G. AC-DC converters for electrolyzer applications: state of the art and future challenges. Published on 29 May 2020. At *Electronics* 2020, 9, 912; <https://doi.org/10.3390/electronics9060912>
- [7] Alhaj Omar F. A new approach for improving the efficiency of the indirectly coupled photovoltaic-electrolyzer system. Published on 22 December 2022. At Int J Hydrogen Energy 48 (2023) 8768 e8782. <https://doi.org/10.1016/j.ijhydene.2022.11.327>
- [8] Alonge F, Collura Stefania Maria, D’Ippolito Filippo, Guilbert D, Luna M, Vitale G. Design of a robust controller for DC/DC converter–electrolyzer systems supplied by  $\mu$ WECSs subject to highly fluctuating wind speed. Published on 10 March 2020. At Control Engineering Practice 98 (2020) 104383.

<https://doi.org/10.1016/j.conengprac.2020.104383>

- [9] Galal Al-Muthanna, Shuhua Fang, Ibrahim AL-Wesabi, Khaled Ameur, Hossam Kotb, Kareem M. AboRas. Design and analysis of A High Speed MPPT Control Utilizing a Hybrid PSO-PID Controller under Partially Shaded Photovoltaic Battery Chargers. Published on 15 February 2023. At *Sustainability* **2023**, *15*, 3578.  
<https://doi.org/10.3390/su15043578>
- [10] Bilal Taghezouit, Fouzi Harrou, Ying Sun and Walid Merrouche. Model-based fault detection in photovoltaic systems: A comprehensive review and avenues for enhancement. Published on 24 January 2024. At *Results in Engineering* **21** (2024) 101835. <https://doi.org/10.1016/j.rineng.2024.101835>.
- [11] Dhanraj J, Mostafaeipour A, Velmurugan K.; Techato K., Chaurasiya P.K., Solomon J.M., Gopalan A, Phoungthong K. An Effective Evaluation on Fault Detection in Solar Panels. Published on 19 November 2021. At *Energies* **2021**, *14*, 7770. <https://doi.org/10.3390/en14227770>.
- [12] Suresh Muthusamy. Fault Detection and Monitoring of Solar PV Panels using Internet of Things. Published on 30.06.2018. At *International Journal of Industrial Engineering*, **2018;2(6)**:146-149. **ISSN: 2456-8449**.  
<https://www.researchgate.net/publication/326913629>.
- [13] Peter Makeen, Hani A. Ghali and Saim Memon. Theoretical and Experimental Analysis of a New Intelligent Charging Controller for Off-Board Electric Vehicles Using PV Standalone System Represented by a Small-Scale Lithium-Ion Battery. Published on 16 June 2022. At *Sustainability* **2022**, *14*, 7396.  
<https://doi.org/10.3390/su14127396>.

## **CHAPTER 8**

### **Acknowledgments**

I would like to express my sincere gratitude to Prof. Anil Kumar Naik, Assistant Professor, Department of Electrical Engineering, for their invaluable guidance and support throughout my internship project. I am also thankful to Prof. Leela Manohar Aeshala, Associate Professor, Department of Chemical Engineering for their constant encouragement and support.

I extend my thanks to Mr. Sudhakar, PHD Scholar, Department of Electrical Engineering for their cooperation and assistance during my internship period. Their support made this project a valuable learning experience.

Tatipamula Chakrapani  
24CHM3R02

1. Prof. Anil Kumar Naik, Assistant Professor, Department of Electrical Engineering
2. Mr. Sudhakar, PHD Scholar, Department of Electrical Engineering
3. Prof. Leela Manohar Aeshala, Associate Professor, Department of Chemical Engineering